

P300 regulates histone crotonylation and preimplantation embryo development

Received: 30 August 2023

Accepted: 19 July 2024

Published online: 30 July 2024

 Check for updates

Di Gao^{1,2,3,5}, Chao Li^{3,5}, Shao-Yuan Liu^{3,5}, Teng-Teng Xu^{4,5}, Xiao-Ting Lin³, Yong-Peng Tan³, Fu-Min Gao³, Li-Tao Yi³, Jian V. Zhang², Jun-Yu Ma³, Tie-Gang Meng³, William S. B. Yeung¹, Kui Liu¹, Xiang-Hong Ou³✉, Rui-Bao Su³✉ & Qing-Yuan Sun³✉

Histone lysine crotonylation, an evolutionarily conserved modification differing from acetylation, exerts pivotal control over diverse biological processes. Among these are gene transcriptional regulation, spermatogenesis, and cell cycle processes. However, the dynamic changes and functions of histone crotonylation in preimplantation embryonic development in mammals remain unclear. Here, we show that the transcription coactivator P300 functions as a writer of histone crotonylation during embryonic development. Depletion of P300 results in significant developmental defects and dysregulation of the transcriptome of embryos. Importantly, we demonstrate that P300 catalyzes the crotonylation of histone, directly stimulating transcription and regulating gene expression, thereby ensuring successful progression of embryo development up to the blastocyst stage. Moreover, the modification of histone H3 lysine 18 crotonylation (H3K18cr) is primarily localized to active promoter regions. This modification serves as a distinctive epigenetic indicator of crucial transcriptional regulators, facilitating the activation of gene transcription. Together, our results propose a model wherein P300-mediated histone crotonylation plays a crucial role in regulating the fate of embryonic development.

Dramatic epigenetic remodeling occurs during early embryonic development, leading to the formation of a totipotent embryo from terminally differentiated gametes^{1,2}. Epigenetic information plays a crucial role in the control of gene expression and the first cell-fate decision during preimplantation embryo development. Aberrant epigenome resetting severely impairs embryo development and even leads to embryonic lethality^{3,4}. Histone modifications, one of the most extensively studied post-translational modifications (PTMs) of histones, are key components of the epigenetic code⁵. They facilitate

nucleosome eviction by disrupting interactions between DNA and histones and promoting RNA polymerase II (RNA Pol II) binding to proximal promoters through recognition of reader proteins^{6–8}. Histone modifications are involved in diverse biological processes, including cell differentiation, zygotic genome activation (ZGA), transcription, and embryonic development^{9,10}. Recent progress in high-resolution liquid chromatography with tandem mass spectrometry (LC-MS/MS) techniques has facilitated the exploration of diverse histone lysine acylation modifications. These encompass histone

¹Shenzhen Key Laboratory of Fertility Regulation, Center of Assisted Reproduction and Embryology, The University of Hong Kong Shenzhen Hospital, 518053 Shenzhen, China. ²Center for Energy Metabolism and Reproduction, Shenzhen Institute of Advanced Technology, Chinese Academy of Sciences, 518055 Shenzhen, China. ³Guangzhou Key Laboratory of Metabolic Diseases and Reproductive Health, Guangdong-Hong Kong Metabolism & Reproduction Joint Laboratory, Reproductive Medicine Center, Guangdong Second Provincial General Hospital, 510317 Guangzhou, China. ⁴MOE Key Laboratory of Gene Function and Regulation, State Key Laboratory of Biocontrol, School of Life Sciences, Sun Yat-sen University, 510275 Guangzhou, China. ⁵These authors contributed equally: Di Gao, Chao Li, Shao-Yuan Liu, Teng-Teng Xu. ✉e-mail: ouxh@gd2h.org.cn; suruihao2022@163.com; sunqy@gd2h.org.cn

butyrylation (Kub), glutarylation (Kglu), β -hydroxybutyrylation (Kbhb), succinylation (Ksucc), lactylation (Kla), and crotonylation (Kcr)^{11,12}. Noteworthy among these modifications is histone crotonylation, which has garnered considerable attention due to its pivotal involvement in transcriptional regulation^{13–15}.

Histone crotonylation modification is predominantly enriched in transcriptional start sites (TSS) and enhancer regions in the mammalian genome. In contrast to histone lysine acetylation (Kac), which exerts a more potent impact on transcriptional activity^{13,14}, most studies have shown that histone crotonylation occurs at gene promoters, suggesting its potential role in facilitating gene transcription^{16–18}. Since the discovery of histone crotonylation, several regulatory enzymes involved in histone crotonylation modifications have been described. In mammalian cells, the transcriptional coactivator P300 possesses histone crotonyltransferase (HCT) activity, catalyzing the crotonylation of histones and directly stimulating the transcription of genes¹⁴. Previous studies have demonstrated that P300 mutants with deficient histone acetyltransferase (HAT) activity but competent HCT activity can substitute for endogenous P300 to enhance transcriptional activation^{19,20}. Furthermore, the intracellular concentration of crotonyl-CoA, regulated by crotonate, directly and positively influences histone crotonylation levels^{14,16,21}. Recent studies have found that histone crotonylation modifications are predominantly involved in spermatogenesis, self-renewal of mouse embryonic stem cells, and mesodermal commitment of human embryonic stem cells in the field of reproduction^{16,22–24}. However, the distribution and function of histone crotonylation in preimplantation embryos remain largely unknown.

In this study, we investigated the distribution of histone crotonylation modifications in embryos at different developmental stages and identified P300 as a key writer of histone crotonylation crucial for embryonic development. We demonstrated that histone crotonylation modifications were involved in the regulation of preimplantation embryo development. Importantly, we found that histone 3 lysine 18 crotonylation (H3K18cr) was specifically enriched at promoter regions in the mammalian genome and positively correlated with gene transcription. During embryonic development, the levels of H3K18cr modification were significantly decreased in the P300 knockdown embryos. Collectively, our results indicate that P300 mediates H3K18cr modification to control the preimplantation embryo development by modulating the transcription of genomes in *mouse* embryos.

Results

P300 is required for early embryonic development

To investigate the regulatory role of P300 during early embryonic development, we performed a comparative analysis of P300 and enzymes with similar functions, including Cbp, Hbo1, and Mof, which are candidate enzymes with HAT and HCT activities, using publicly available single-cell RNA-sequencing (scRNA-seq) datasets²⁵. Through comparative analysis of FPKM values in embryos at different developmental stages, we found that *P300* exhibits the most dramatic expression changes compared to several other candidate genes, particularly during the period from fertilization to the four-cell stage. *P300* expression displayed a pronounced decline in subsequent developmental stages, from the 8-cell phase onward, consistently decreasing until the blastocyst stage (Fig. 1a). Consistent with the RNA sequencing results, qPCR analysis showed a similar expression pattern of *P300* in preimplantation embryos (Fig. 1b). Immunofluorescence staining confirmed a nuclear localization of P300 protein in embryos of different developmental stages, with an increase in P300 intensity after fertilization (Fig. 1c, d). These findings imply that P300 may play a critical role during early embryonic development.

To further investigate the function of P300 in embryonic development, we performed P300 knockdown experiments using P300-

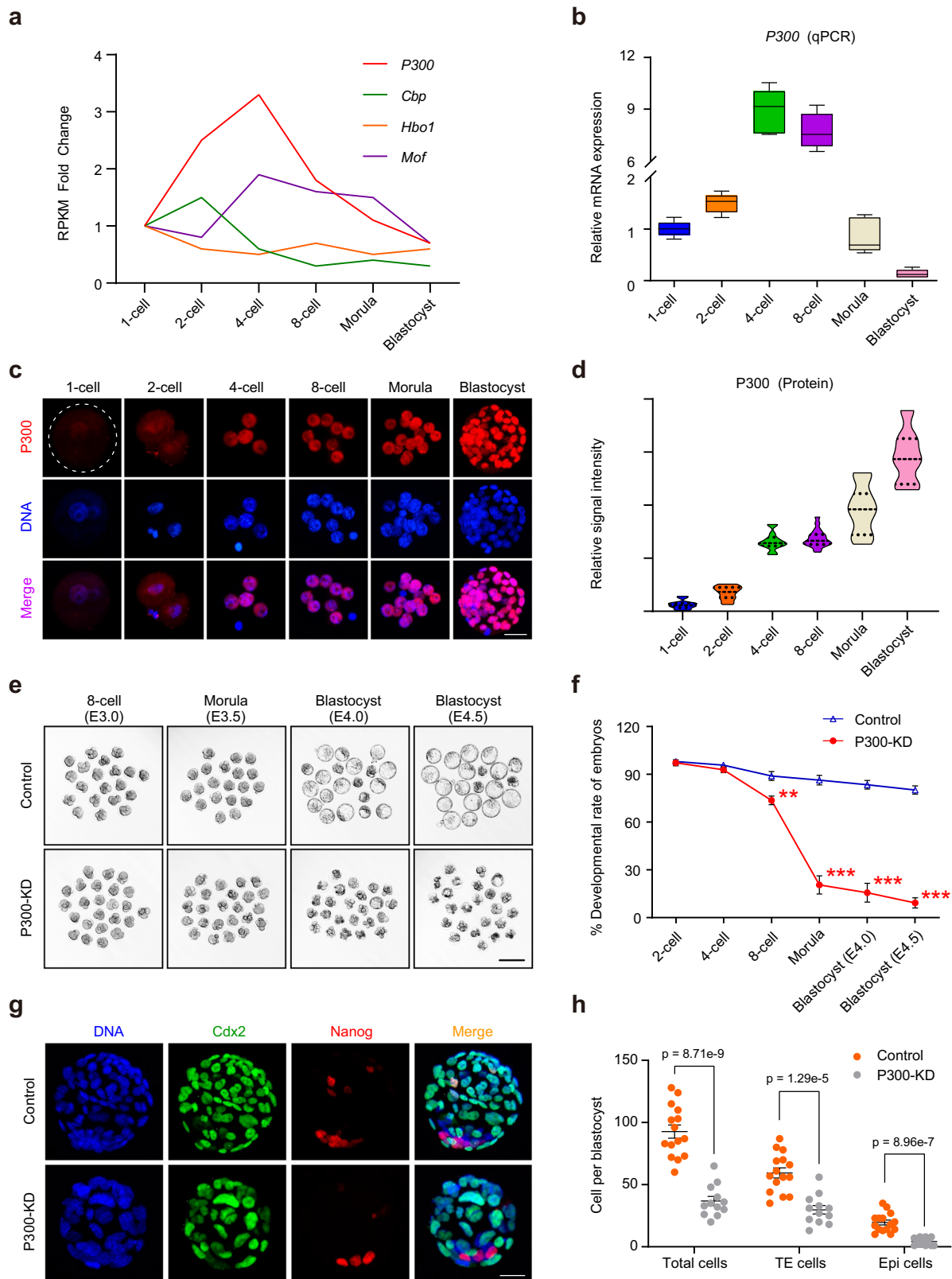
targeted siRNA. Microinjection of P300 siRNA into the cytoplasm of early zygotes resulted in a significant decrease in *P300* mRNA levels across multiple developmental stages, including 4-cell, 8-cell, morula, and blastocyst (Supplementary Fig. 1a). Immunofluorescence staining and western blotting confirmed the reduction of P300 protein in 8-cell embryos (Supplementary Fig. 1b, c). We then assessed the developmental competence of the embryos after P300 knockdown. The results displayed that early cleavage of embryos remained unaffected upon P300 knockdown. However, a notable decline in developmental efficiency from the 8-cell stage onward ($P < 0.05$, Fig. 1e, f), particularly affecting the 8-cell to morula transition was observed. Notably, a large proportion of the P300 knockdown embryos exhibited developmental arrest at the 8-cell stage (62%), whereas the control embryos demonstrated a robust progression, with 80% successfully advancing to the blastocyst stage (Fig. 1f).

The quality of the blastocyst is a crucial factor in assessing successful embryo implantation. Therefore, we examined the cell counts of whole embryo, trophoblast cells (TE), and epiblast cells (Epi) in blastocysts to determine their quality. Immunostaining of blastocysts with DAPI, CDX2, and NANOG antibodies allowed quantification of total cells, TE cells, and Epi cells, respectively (Fig. 1g). The findings revealed a noteworthy decrease in these cell counts in the P300 knockdown embryos (Fig. 1h). Furthermore, to investigate the role of P300 after ZGA, we depleted P300 by injecting P300 siRNA into the two-cell blastomeres during the late 2-cell stage (Supplementary Fig. 2a). Consistently, the phenotype observed in the siRNA-mediated P300 knockdown embryos was similar to that observed in embryos injected at the zygote stage (Supplementary Fig. 2b, c), suggesting that P300 is also involved in early embryonic development after ZGA. Together, these findings demonstrate the essential requirement of P300 for preimplantation embryonic development in mice.

P300 knockdown results in an aberrant gene expression pattern of embryos

To understand the molecular basis of the developmental failure observed in the P300 knockdown embryos, we performed total RNA-seq experiments comparing the control and the P300 knockdown embryos (Fig. 2a). A strong correlation was observed among two biological replicates of RNA-seq samples from each group (Supplementary Fig. 3a, b), thus confirming the precision of the acquired gene expression profiles (Fig. 2b). We first analyzed the transcriptome data from late 2-cell stage embryos to investigate whether knockdown of P300 would affect the ZGA. Sequencing results showed that knockdown of P300 resulted in changes in the expression of 296 genes, with 206 upregulated and 90 downregulated (Supplementary Fig. 3c). Next, we performed enrichment analysis of these differentially expressed genes with identified minor ZGA and major ZGA genes²⁶. The results showed that only 15 minor ZGA genes and 92 major ZGA genes exhibited altered expression (Supplementary Fig. 3c and Supplementary Data 1), indicating that the dysregulation of genes related to ZGA may not be the primary cause of the 8-cell arrest.

From the 4-cell to late 8-cell stages, we selected mRNAs possessing dependable sequence annotations and fragments per kilobase of transcript per million mapped reads (FPKM > 1) for subsequent analysis (Fig. 2a). Among the 11,019 transcripts analyzed, we categorized them into eight clusters: from Cluster I to Cluster VIII (Fig. 2c). Cluster I represented mRNAs that were continuously transcribed, while Cluster II showed the exact opposite pattern. Clusters III to Clusters VIII contain mRNA transcripts that exhibit different expression patterns, showing varying degrees of upregulation or downregulation. Upon analyzing the RNA-seq outcomes encompassing the 4-cell to late 8-cell embryonic stages, a large number of genes were dysregulated in the P300 knockdown group when compared with the control group. Among these, the expression levels of transcripts in Clusters I, Clusters V, and Clusters VI gradually increased in the control group. However,



the trend of transcripts upregulation becomes less pronounced after P300 knockdown. In contrast, some transcripts in Cluster II, Clusters III, Clusters VII, and Cluster VIII did not show the normal degradation pattern (Fig. 2c). These findings suggest that the abnormal expression of genes during the 4-cell to late 8-cell developmental stage induced by P300 knockdown may be the main cause of inhibition of embryonic development.

We further examined the differentially expressed genes (DEGs) between the control and the P300 knockdown embryos. Compared to the control group, in the 4-cell stage embryos, the P300 knockdown group exhibited 418 upregulated genes and 419 downregulated genes ($P_{\text{adj}} \leq 0.05$; fold change ≥ 1.5). In contrast, at the late 8-cell stage, a total of 4697 genes were differentially expressed, with 2483 upregulated and 2214 downregulated genes (Fig. 2d and Supplementary

Fig. 1 | P300 is essential for preimplantation development. **a** Line plots showing the mRNA profiles of *P300*, *Cbp*, *Hbo1*, and *Mof* in various developmental stages of mouse preimplantation embryos were examined by RNA-seq. **b** Quantitative PCR analysis of relative *P300* expression levels in embryos at different developmental stages. The experiment was conducted with five independent biological replicates, and *H2afz* was used as the reference gene. The center line and edges of the boxes represent the median and quartiles of the data points, respectively. The minimum and maximum values in the boxplots correspond to quartile 1 – 1.5 × interquartile range and quartile 3 + 1.5 × interquartile range, respectively. **c** Immunostaining of P300 (red) at the individual developmental stage. 1-cell ($n = 13$); 2-cell ($n = 11$); 4-cell ($n = 12$); 8-cell ($n = 15$); morula ($n = 15$); blastocyst ($n = 14$). Scale bar: 50 μm . **d** Relative P300 intensity compared to the 1-cell stage. Data are presented as mean values \pm SEM. **e** Representative images of embryonic development from the 8-cell stage to the blastocyst stage. P300 siRNA was injected into the zygotes as the experimental group ($n = 148$), while a negative control siRNA was used as the

control group ($n = 157$). Scale bar: 100 μm . **f** Statistical analysis of the impact of P300 siRNA injection on embryonic development rate. $n = 7$ biological replicates. Data are presented as mean values \pm SEM. Statistical analysis was performed using two-tailed unpaired *t*-tests. Developmental stages: 2-cell ($P = 0.75$), 4-cell ($P = 0.27$), 8-cell ($P = 2.35\text{e-}3$), Morula ($P = 2.75\text{e-}7$), Blastocyst E4.0 ($P = 4.07\text{e-}6$) Blastocyst E4.5 ($P = 9.25\text{e-}10$) for P300-KD (P300 knockdown, red line) vs. control (blue line). ** $P < 0.01$; *** $P < 0.001$. **g** Representative immunofluorescence staining images for Cdx2 and Nanog in control and P300 knockdown blastocysts at 4.5dpc, based on three independent experiments. Scale bar: 20 μm . **h** Dot plots displaying the average counts of total cells, TE cells, and Epi cells per blastocyst embryo in control and P300 siRNA-treated embryos at 4.5dpc. $n = 3$ biological replicates. TE, trophectoderm. Epi, epiblast. The number of blastocysts in the control group and the P300-KD group were 15 and 12, respectively. Data are presented as mean values \pm SEM and were analyzed using two-tailed unpaired *t*-tests.

Data 1). To further understand the function of DEGs, we conducted gene ontology (GO) analysis. The analysis yielded notable enrichment of terms associated with the embryonic development and cellular metabolic processes among the downregulated DEGs (Fig. 2e). Notably, the downregulated genes were associated with cellular amino acid metabolic process, regulation of oxidative phosphorylation, blastocyst formation and development, and tight junction assembly, which are known markers associated with embryo development and cell metabolism. In the set of DEGs, a substantial decrease in gene expression levels of vital transcription factors associated with embryonic development, including *Nanog*, *Pou5f1*, *Cdx2*, *Myc*, *Tbx3*, *Gata3*, *Gata6*, *Klf5*, and *Klf8* (Fig. 2f–i). Furthermore, transcriptomic data revealed a significant downregulation of genes associated with tight junction assembly among these downregulated DEGs. Subsequently, we examined the relevant genes mentioned above and confirmed that the knockdown of P300 markedly reduced the expression levels of genes associated with tight junction assembly, including *Cdh1*, *Ocln*, *Cldn4*, and *Cldn7* (Fig. 2f, j). Moreover, knockdown of P300 also notably decreased the expression levels of genes related to cytoskeleton and fluid accumulation, such as *F11r*, *Prkcz*, *Aqp3*, and *Aqp9* (Supplementary Fig. 3d). Considering the developmental phenotype observed in previous studies, we propose that in P300 knockdown embryos at the late 8-cell stage, the dysregulation of genes associated with embryonic development and the failure of tight junction assembly events may be significant reasons for embryo failure to transit from the 8-cell to the morula stage. Overall, our results suggest that P300 plays a critical role in modulating gene expression involved in embryonic development.

P300 is involved in regulating the transcription elongation of RNA polymerase II

Our findings have demonstrated that P300 knockdown results in widespread dysregulation of gene expression, particularly downregulation of gene expression. Therefore, we examined the transcriptional activities of RNA using EU staining. The results indicated that transcriptional activation in late 8-cell embryos was significantly compromised after P300 knockdown (Fig. 3a). However, there was no change in transcriptional activity in embryos at the 2-cell and 4-cell stages following P300 knockdown. (Supplementary Fig. 4a, b). Gene ontology analysis revealed a significant inhibition of the function of transcription elongation of RNA Pol II after P300 knockdown (Fig. 2e). To investigate the potential impact of P300 knockdown on the genome-wide transcriptional elongation program, we evaluated the levels of phosphorylated Ser2 (Ser2P), a characteristic indicator of RNA Pol II activity. In alignment with our initial hypothesis, a considerable decline in the Ser2P protein levels was observed in the P300 knockdown embryos during the late 8-cell stage (Fig. 3b, c). Additionally, the Ser2P levels exhibited no significant disparity within the P300 knockdown embryos during the 2-cell stage (Supplementary Fig. 4c, d) and displayed a subtle decrease during the 4-cell stage (Supplementary

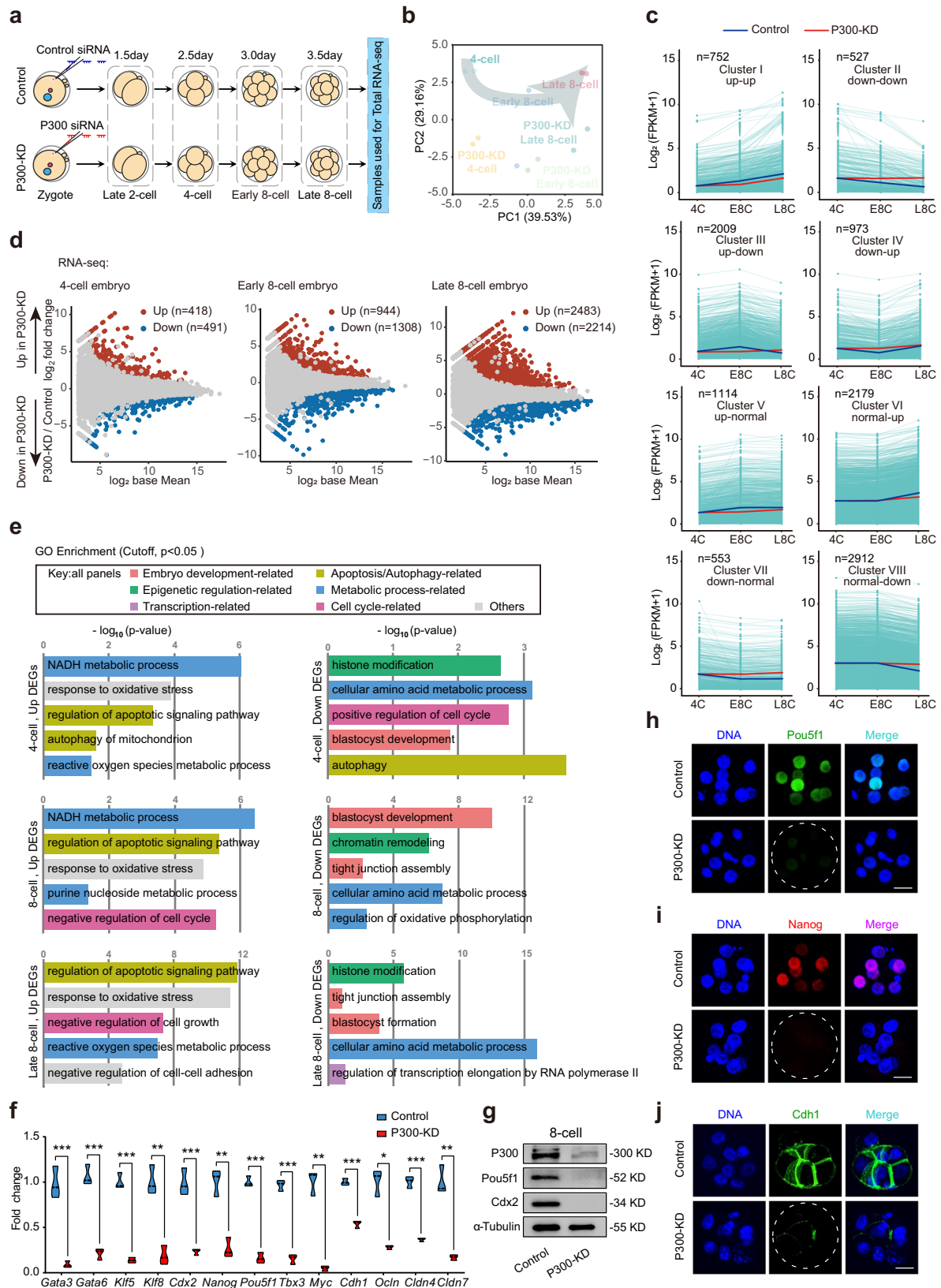
Fig. 4e, f). Collectively, P300 knockdown impairs RNA transcription and the transcription elongation of RNA Pol II at the late 8-cell stage.

We also performed CUT&Tag assays using Pol II antibody on both control and P300 knockdown embryos during the late 8-cell stage (Fig. 3d). To evaluate our CUT&Tag technique, we compared the number of relevant peaks, peak distribution, and the correlation between data using publicly available Stacc-seq data for RNA Pol II and CUT&RUN data for H3K27ac^{7,26}. As expected, our method closely resembled the high-quality published data, with some metrics even showing superior performance, thus facilitating subsequent experimental analyses (Supplementary Fig. 5a–h). Hierarchical clustering and Pearson correlation analyses demonstrated a high correlation between the Pol II CUT&Tag data from the P300 knockdown embryos and the control group (Supplementary Fig. 5i–k). Based on the changes in transcripts observed in the RNA-seq data, we categorized the Pol II peaks in gene body regions into three types in the control group. We found that the signal of Pol II was significantly shifted upwards in the upregulated genes compared to the unchanged genes and significantly shifted downwards in the downregulated genes (Fig. 3e), suggesting that there might be a positive correlation between Pol II occupancy and transcript changes. Next, we examined the correlation between gene expression alterations and Pol II occupancy after P300 knockdown (Fig. 3f). Remarkably, for the upregulated transcripts, there was a notable elevation in the Pol II signal in the P300 knockdown embryos as compared to the control group (Fig. 3g). In contrast, the signal of Pol II was markedly decreased in the downregulated transcripts, while no visible difference was observed in unaffected transcripts between the P300 knockdown and the control groups (Fig. 3h, i). A representative track view further supported these findings (Fig. 3j). For example, the Pol II peaks of the *Hmox1* gene were dramatically increased in the P300 knockdown embryos from the transcription start site (TSS) to transcription end site (TES), while the *Pou5f1* gene displayed an opposite enrichment pattern. These results confirm that the Pol II signals are positively correlated with transcript changes following P300 knockdown during embryonic development.

P300 catalyzes site-specific histone lysine crotonylation in embryos

Previous studies have shown that P300 mediates H3K27ac modification to regulate preimplantation embryonic development²⁶. To further demonstrate the role of P300 in histone acetylation, we also examined the expression levels of H3K27ac and H3K9ac. Immunofluorescence and Western blot results showed no appreciable changes in H3K9ac modification levels (Supplementary Fig. 6a), while a substantial reduction in H3K27ac levels in the P300 knockdown embryos compared to the control (Supplementary Fig. 6b, c). These findings are consistent with previous research²⁶.

Recent studies have proposed a role for histone crotonylation in promoting the differentiation of human embryonic stem cells into



endoderm^{16,24}, suggesting a potential conservation of histone crotonylation during preimplantation embryonic development. To assess this hypothesis, we examined the dynamic intensity of histone crotonylation during early embryo development using immunofluorescence staining. The results revealed the presence of histone crotonylation modification in different developmental stages of

mouse embryos (Supplementary Fig. 6d), with crotonylation levels significantly increasing from the 8-cell to the blastocyst stage, indicating the importance of histone crotonylation in blastocyst formation. As the transcriptional coactivator P300 possesses HCT activity and is a key writer of crotonylation modification^{14,27}, we thus investigated whether the levels of histone crotonylation were altered in the

Fig. 2 | P300 plays a critical role in determining the gene expression of pre-implantation embryos. **a** Diagram illustrating the procedure of acquiring samples for total RNA-seq analysis in embryos subjected to P300 knockdown (P300-KD) and control conditions. **b** Bidimensional principal-component (PC) analysis was conducted to assess the gene expression patterns in embryos undergoing pre-implantation development under control and P300 knockdown conditions. **c** Expression patterns of mouse genomic transcripts from the 4-cell to late 8-cell stages in preimplantation embryos derived from control and P300 knockdown embryos. Individual gene expression levels are depicted by the light green lines, while the median expression levels of the group are indicated by the central red and blue lines. Analysis was focused on transcripts with FPKM > 1 at the 4-cell stage. 4 C, E8C, and L8C represent embryos at the 4-cell, early 8-cell, and late 8-cell stages, respectively. **d** Scatter plots illustrate the RNA-seq-based analysis of differential gene expression in embryos at the 4-cell, early 8-cell, and late 8-cell stages after P300 knockdown. The criteria for significance were fold change $\geq |1.5|$ and an adjusted P value (P_{adj}) < 0.05. **e** GO analysis of differentially expressed genes (DEGs)

in P300 knockdown embryos, assessed by enrichment. **f** Expression patterns of functional genes involved in embryo development and tight junction assembly were visualized using violin plots for both the control and P300 knockdown groups. Data are presented as mean values \pm SEM. $n = 3$ biological replicates. *H2afz* was used as the reference gene. *Gata3* ($P = 1.03e-3$), *Gata6* ($P = 3.57e-4$), *Klf5* ($P = 9.70e-5$), *Klf8* ($P = 1.88e-3$), *Cdx2* ($P = 1.03e-3$), *Nanog* ($P = 2.33e-3$), *Pou5f1* ($P = 6.68e-5$), *Tbx3* ($P = 7.19e-5$), *Myc* ($P = 5.30e-3$), *Cdh1* ($P = 1.60e-4$), *Ocln* ($P = 0.01$), *Cldn4* ($P = 9.15e-5$), *Cldn7* ($9.74e-3$). * $P < 0.05$; ** $P < 0.01$; *** $P < 0.001$. **g** Western blot analyses were conducted to assess Pou5f1 and Cdx2 protein levels in both the control and P300 knockdown embryos at the late 8-cell stage. Each group consisted of 100 embryos, and the experiment was repeated twice, yielding consistent outcomes. α -Tubulin served as the control for normalization. **h–j** Representative images of immunofluorescence staining for Pou5f1 (**h**), Nanog (**i**), and Cdh1 (**j**) in control and P300 knockdown embryos at the late 8-cell stage. Scale bar: 20 μ m. In (**d**), (**e**), and (**f**), statistical analysis was performed using two-tailed unpaired t -tests.

P300 knockdown embryos (Fig. 4a). A noticeable decrease in the levels of histone crotonylation modification was observed in the P300 knockdown embryos in comparison to the control group (Fig. 4i), confirming the role of P300 as the major HCT during mammalian embryonic development.

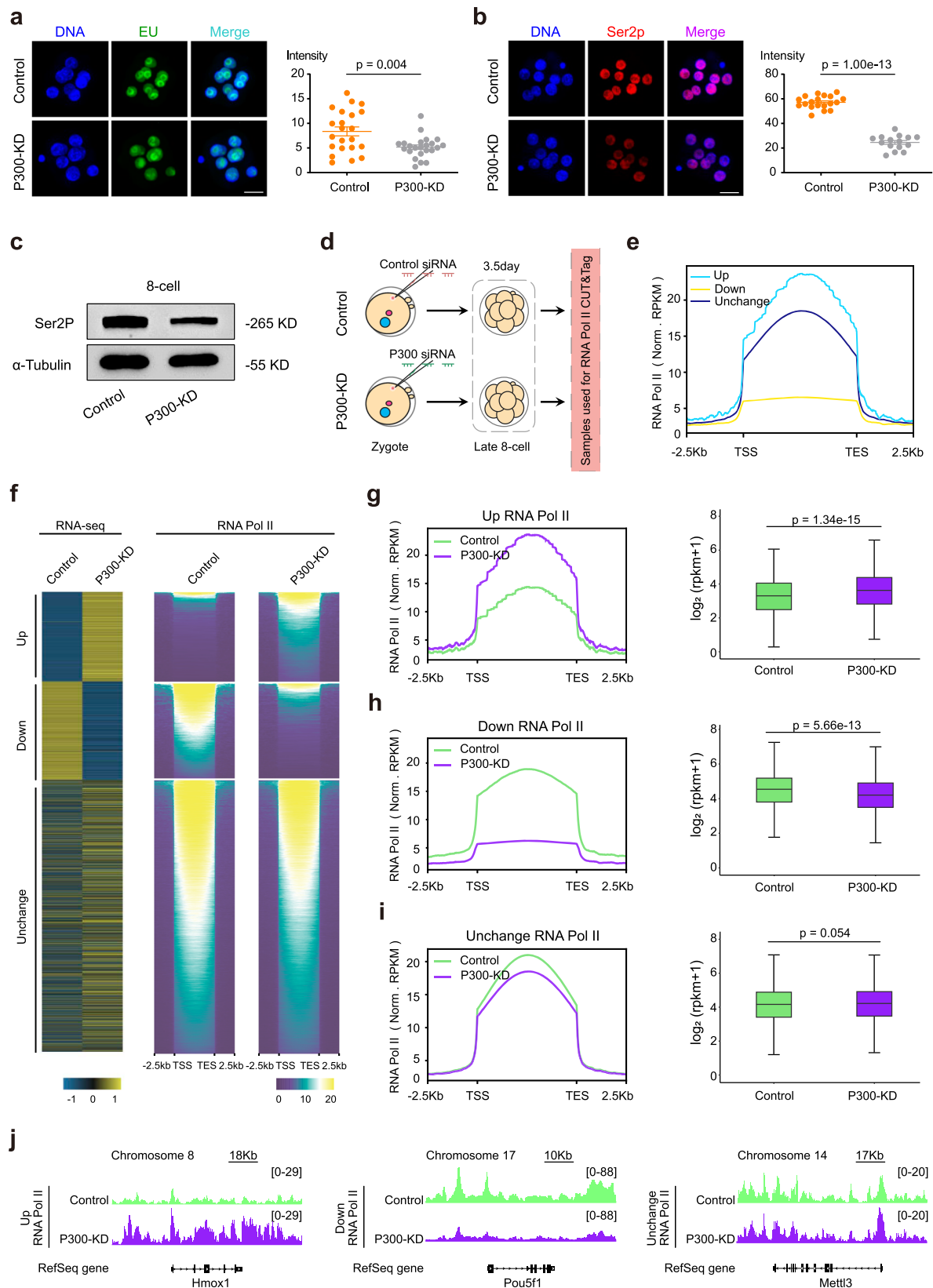
Next, we examined the site specificity of histone crotonylation catalyzed by P300. Our results demonstrated that P300 was active for most of the tested sites, including H3K18cr, H3K9cr, H3K23cr, H3K36cr, H3K27cr, H3K14cr, and H4K12cr (Fig. 4b–i). The Western blot analysis provided additional validation for the observation (Fig. 4j). Regarding the partial discrepancies observed between the data obtained by the two aforementioned methods, we speculate that these differences may stem from variations in antibody efficiency and specificity. Nevertheless, the overall changing patterns resulting from P300 knockdown remain consistent between both techniques. Interestingly, the knockdown of P300 in embryos resulted in a significant reduction of the H3K18cr level (Fig. 4b, i) and a moderate reduction of the H3K9cr level (Fig. 4c, i), whereas the modification levels of H3K23cr, H3K36cr, H3K27cr, and H3K14cr were slightly decreased (Fig. 4d–i). Furthermore, the modification level of H4K12cr was not significantly changed in the P300 knockdown embryos (Fig. 4h, i). These findings suggest that the developmental failure observed upon P300 knockdown may be attributed to aberrant histone crotonylation, particularly H3K18cr, during embryonic development. In summary, our data demonstrate that P300 acts as an HCT with distinctly modified lysine residue in the preimplantation embryos.

Histone lysine crotonylation regulates early embryonic development

To further explore the contribution of histone lysine crotonylation in early embryonic development, we attempted to rescue the P300 knockdown embryos using mutants with crotonylation function. Based on the reported P300 and acetyl-CoA co-structure²⁸, we focused on the isoleucine residue 1394 mutation (Fig. 5a), generating a P300-I1394G mutant. This variant is characterized by impaired HAT activity while retaining HCT function (Supplementary Fig. 7a–c), in accordance with previous research accounts¹⁹. We injected zygote embryos with the P300-I1394G mutant mRNA, and found no effect on embryo development (Supplementary Fig. 7d, e). Using the P300-I1394G mutant mRNA with crotonylation function, we then tried to rescue the development of P300 knockdown embryos (Fig. 5b). Our results revealed that P300 knockdown zygote embryos injected with P300-I1394G mutant mRNA partially restored embryonic development (Fig. 5c, d). While the extent of histone crotonylation in the rescue embryos at the morula stage did not fully match that of the control, a noteworthy enhancement in Kcr modification levels was observed compared to the P300 knockdown group (Fig. 5e). Moreover, the restoration of histone crotonylation to normal levels was evident in the

rescue group embryos that successfully developed to the blastocyst stage (Fig. 5f). To ensure the efficiency of P300 degradation at different stages and to eliminate interference from acetylation after rescue, we collected embryos from the 2-cell to 8-cell stages in the control, knockdown, and rescue groups, and then measured the expression levels of P300 and H3K27ac. The results showed a significant decrease in P300 expression levels from the 2-cell to 8-cell embryos in the P300 siRNA group. Conversely, the expression of the exogenous P300-I1394G mutant in the rescue group was significantly enhanced, while the expression of H3K27ac remained at a lower level after rescue (Supplementary Fig. 8a–e). Additionally, we employed samples rescued after supplementation as positive controls and assessed the levels of H3K18cr modification. The results revealed a notable increase in H3K18cr modification levels after supplementation with the P300 mutant. To validate the regulatory role of P300 as a crotonylation modification enzyme on lysine residues, we evaluated the crotonylation levels on histone lysine residues in P300 knockout mouse embryonic stem cells (mESC). Strikingly, our study demonstrated that the deletion of P300 significantly reduced the levels of crotonylation modifications at H3K9, H3K14, H3K18, H3K23, H3K27, and H3K36 sites (Supplementary Fig. 8g). Upon overexpression the P300 mutant into the P300 knockout cell line, crotonylation levels at the H3K18 and H3K9 sites significantly increased, with H3K18 exhibiting the most pronounced change. Additionally, there was a slight increase in crotonylation levels at H3K14, H3K23, H3K27, and H3K36 sites, while the level of H3K27ac remained unchanged (Supplementary Fig. 8g). These results were consistent with those observed in mouse embryos (Fig. 4). In summary, these findings underscore the indispensable role of appropriate histone crotonylation expression in preimplantation embryonic development.

Crotonate (NaCr) is a short-chain fatty acid (SCFA) precursor of crotonyl-CoA. Supplementation with crotonate has been shown to dramatically enhance cellular levels of crotonyl-CoA and histone crotonylation, leading to increased gene expression in vivo and in vitro^{14,20,23}. Mechanistically, NaCr generates crotonyl-CoA, which in turn catalyzes the crotonylation of histones in cells (Fig. 5g). Therefore, we also attempted to rescue the development of P300 knockdown embryos by supplementing the KSOM medium with NaCr (Fig. 5h). After successfully demonstrating that P300 siRNA effectively silenced P300 protein in embryos from the 2-cell to 8-cell stages (Supplementary Fig. 8a–e), we discovered that supplementation with 10 μ M NaCr enabled the majority of P300 knockdown embryos to overcome the 8-cell block (Fig. 5i). Specifically, 58% of the embryos developed to the morula stage, and 36% even reached the blastocyst stage (Fig. 5j). To assess whether the modification levels of histone crotonylation were restored in the NaCr rescue embryos, we further analyzed the fluorescence signal among the three groups (Fig. 5h). The results showed that the addition of NaCr significantly increased global histone



crotonylation in the P300 knockdown embryos, indicating a restoration of histone crotonylation reprogramming (Fig. 5e). As expected, the levels of histone crotonylation at the blastocyst stage were also restored to normal in the rescue group (Fig. 5k). To further eliminate interference from acetylation in the NaCr rescue group, we collected embryo samples from the 2-cell to 8-cell stages to assess the

expression levels of H3K27ac and Kac, H3K18cr and Kcr as positive controls. The results indicated that the NaCr rescue group only restored the modification levels of Kcr and H3K18cr, without altering the modification levels of Kac and H3K27ac (Supplementary Figs. 8a–e and 9a–e). Furthermore, our findings also suggested that with increasing NaCr concentration in the culture medium, global

Fig. 3 | Effects of p300 knockdown on transcription elongation of RNA polymerase II. **a** Images reveal a substantial decrease in EU-positive nuclear signals in P300 knockdown (P300-KD) embryos at the late 8-cell stage. The nuclei were stained with DAPI (blue). Left: One representative image of EU-positive nuclear signals. Scale bar: 20 μ m. Right: Immunofluorescence analyses of the EU-positive nuclear signals in late 8-cell embryos. $n = 3$ biological replicates. Control ($n = 22$), P300-KD ($n = 23$). **b** Representative images reveal a substantial decrease in Phospho-RNA pol II C-terminal domain (Ser2P) nuclear signals in P300-KD embryos at the late 8-cell stage. The nuclei were stained with DAPI (blue). Left: One representative image of Ser2P signals. Scale bar: 20 μ m. Right: Immunofluorescence analyses of the Ser2P signals in late 8-cell embryos. $n = 3$ biological replicates. Control ($n = 19$), P300-KD ($n = 15$). **c** Western blot analyses were conducted to examine the levels of Ser2P in control and P300-KD embryos. Each group consisted of 100 embryos. $n = 2$ biological replicates. α -Tubulin served as the control for normalization. **d** Schematic of sample collection for Pol II CUT&Tag analysis in

control and P300 knockdown (P300-KD) group. **e** Gene body Pol II enrichment forms the three classes of genes in control and P300-KD embryos. **f** Heatmaps showing the gene body Pol II enrichment and differentially expressed genes in control and P300 knockdown embryos. TSS, transcription start site. TES, transcription end site. **g–i** The average plot showing the knockdown of P300 resulted in widespread alterations of Pol II enrichment (Z-score normalized) at the gene body regions, such as upregulated (**g**, $n = 1396$), downregulated (**h**, $n = 1177$), and unchanged (**i**, $n = 6532$). The center line and edges of the boxes represent the median and quartiles of the data points, respectively. The minimum and maximum values in the boxplots correspond to quartile 1–1.5 \times interquartile range and quartile 3 + 1.5 \times interquartile range, respectively. $n = 2$ biological replicates. **j** Representative tracks showing occupancy of Pol II at the gene body regions of genes (*Hmox1*, *Pou5f1*, and *Mettl3*) in the control and P300-KD embryos (two biological replicates). In (**a**), (**b**), (**g**), (**h**), and (**i**), statistical analysis was performed using two-tailed unpaired *t*-tests. Data are presented as mean values \pm SEM.

levels of Kcr and H3K18cr exhibited a dose-dependent increase (Supplementary Fig. 9f). These results once again demonstrate the requirement of histone crotonylation for proper embryo development.

We also performed a comprehensive total RNA-seq analysis on the two groups of rescued embryos (Fig. 5b, h). We observed a heightened resemblance between the P300-I1394G mutant mRNA rescue, NaCr rescue, and control embryos, through hierarchical clustering and Pearson correlation assessments of the expression patterns of all annotated transcripts (Supplementary Fig. 3e). Two independent replicates showed a high correlation (Supplementary Fig. 3f), indicating that the extensive transcriptional changes observed in the P300-I1394G mutant mRNA rescue and the NaCr rescue embryos at least partially resemble those in the control embryos. In fact, the transcriptomic analysis revealed that the expression of 45.89% of downregulated genes and 55.82% of upregulated genes in the P300 knockdown group could be predominantly corrected by injection of P300-I1394G mutant mRNA (Fig. 5i and Supplementary Data 1). In the NaCr group, the expression of 45.89% of downregulated genes and 66.85% of upregulated genes was corrected, respectively (Fig. 5i and Supplementary Data 1). Supporting this finding, a representative track view demonstrated that the *Nanog* gene loci, which exhibited abnormally low expression levels in the P300 knockdown embryos, showed recovery of expression levels after rescue (Fig. 5m). Similarly, the *Casp2* gene exhibited a noticeable rise in signal intensity in the P300 knockdown embryos when compared with the control group, whereas the signal intensity was dramatically reduced in the rescue groups (Fig. 5m). These results indicate that histone crotonylation modification is involved in the transcriptional regulation of genes. Remarkably, the GO analysis revealed that these rescued transcripts were enriched for functions related to embryo development, epigenetic regulation, and metabolic process including blastocyst development, histone modification, chromatin remodeling, and cellular amino acid metabolic process (Fig. 5n). Additionally, positive regulation of the cell cycle function was also enriched. In summary, these findings indicate that P300-mediated histone crotonylation modification regulates the development of preimplantation embryos by influencing the transcription of key genes that play essential roles during embryonic development stages.

H3K18cr supports preimplantation embryonic development by regulating gene transcripts

The above results have shown that the H3K18cr levels were significantly decreased in the P300 knockdown embryos (Fig. 4b, i). To explore the correlation between H3K18cr modification and dysregulation of gene expression after P300 knockdown, we performed CUT&Tag experiments using an H3K18cr antibody. First, we validated the antibody using mouse embryonic stem cells (mESCs) and mouse embryonic fibroblasts (MEFs) (Supplementary Figs. 8f and 10). The

results showed a prominent enrichment of H3K18cr peaks at promoter regions (Supplementary Fig. 10a, b), and the replicates displayed a high correlation (Supplementary Fig. 10c, d). We further optimized the experimental conditions and obtained the H3K18cr modification profiles using a reduced number of morula embryos. To validate the H3K18cr CUT&Tag data in early embryos, we conducted several analyses. First, a substantial proportion of the H3K18cr peaks were found to be enriched at the promoter regions, similar to the data observed in the MEF cells (Supplementary Fig. 10a, b). Second, the biological replicates of H3K18cr CUT&Tag data were highly reproducible (Supplementary Fig. 10c). Lastly, for developmentally regulated transcription factors such as *Dux*, *Tbx3*, *Gata6*, *Klf5*, and *Klf13*, we observed elevated H3K18cr peak enrichment at annotated promoters during the corresponding developmental stages when these factors are expressed (Supplementary Fig. 10d). These results demonstrate the generation of high-quality H3K18cr CUT&Tag data from early embryos, which can be utilized for subsequent experiments.

To gain further insights into the role of H3K18cr in transcription during preimplantation embryonic development, we performed CUT&Tag assays for H3K18cr in control, P300 knockdown, and rescue group embryos at the late 8-cell stage (Fig. 6a). The results demonstrated a strong correlation between replicates of H3K18cr CUT&Tag data (Supplementary Fig. 11a), with Pearson's correlation coefficients >0.95 , indicating the robust reproducibility of the H3K18cr CUT&Tag data (Supplementary Fig. 11b, c). We subsequently analyzed the target sites and observed that the majority of H3K18cr enrichment sites were located at promoters, intronic regions, and distal intergenic regions (Fig. 6b). Notably, H3K18cr exhibited distinct distribution changes in the P300 knockdown embryos, with decreased enrichment at the promoter regions and increased enrichment at the distal regions (Fig. 6b). Consistent with the RNA-seq results, the H3K18cr-enriched peaks at promoter and distal regions in the rescue group embryos were similar to those in the control group (Fig. 6b). Analyzing the average signal levels of H3K18cr across the entire genome, we consistently observed high levels of H3K18cr at the transcription start site (TSS) regions. Interestingly, the H3K18cr signal at the TSS regions was significantly decreased in the P300 knockdown embryos compared to the control and the rescue groups (Fig. 6c, d). These results suggest that changes in the H3K18cr signal at the TSS regions may be associated with alterations in transcripts following P300 knockdown.

We next sought to determine how H3K18cr contributes to transcription during preimplantation embryonic development. Specifically, we analyzed the H3K18cr-enriched peaks at the TSS regions in each group of embryos. Our results revealed a significant reduction in the H3K18cr peaks at the TSS regions in the P300 knockdown embryos. Remarkably, the number of H3K18cr peaks at the TSS regions increased in the I1394G mutant mRNA rescue and the NaCr rescue group embryos (Fig. 6e, f), suggesting the involvement of P300-mediated H3K18cr modification in the regulation of gene

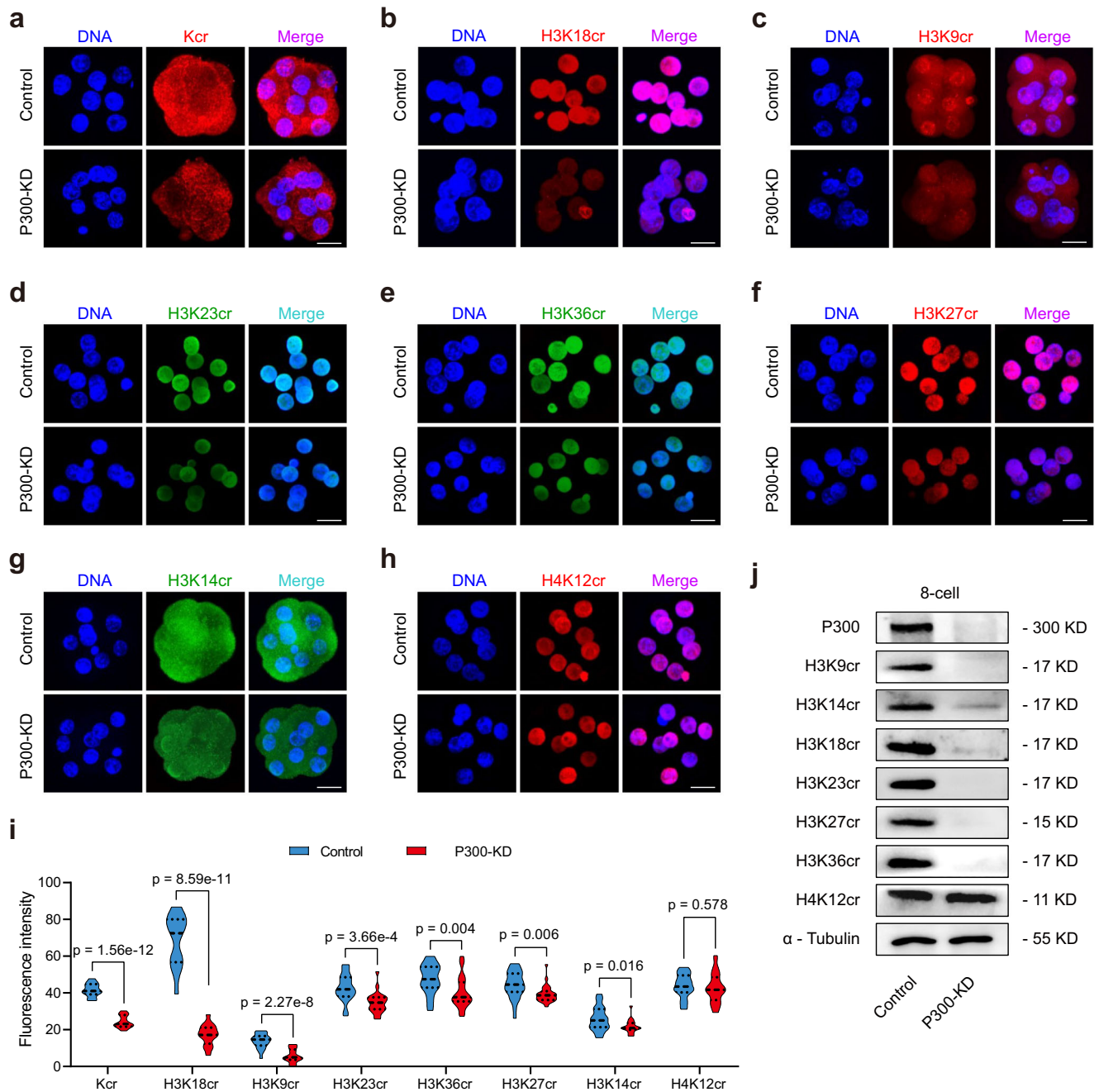


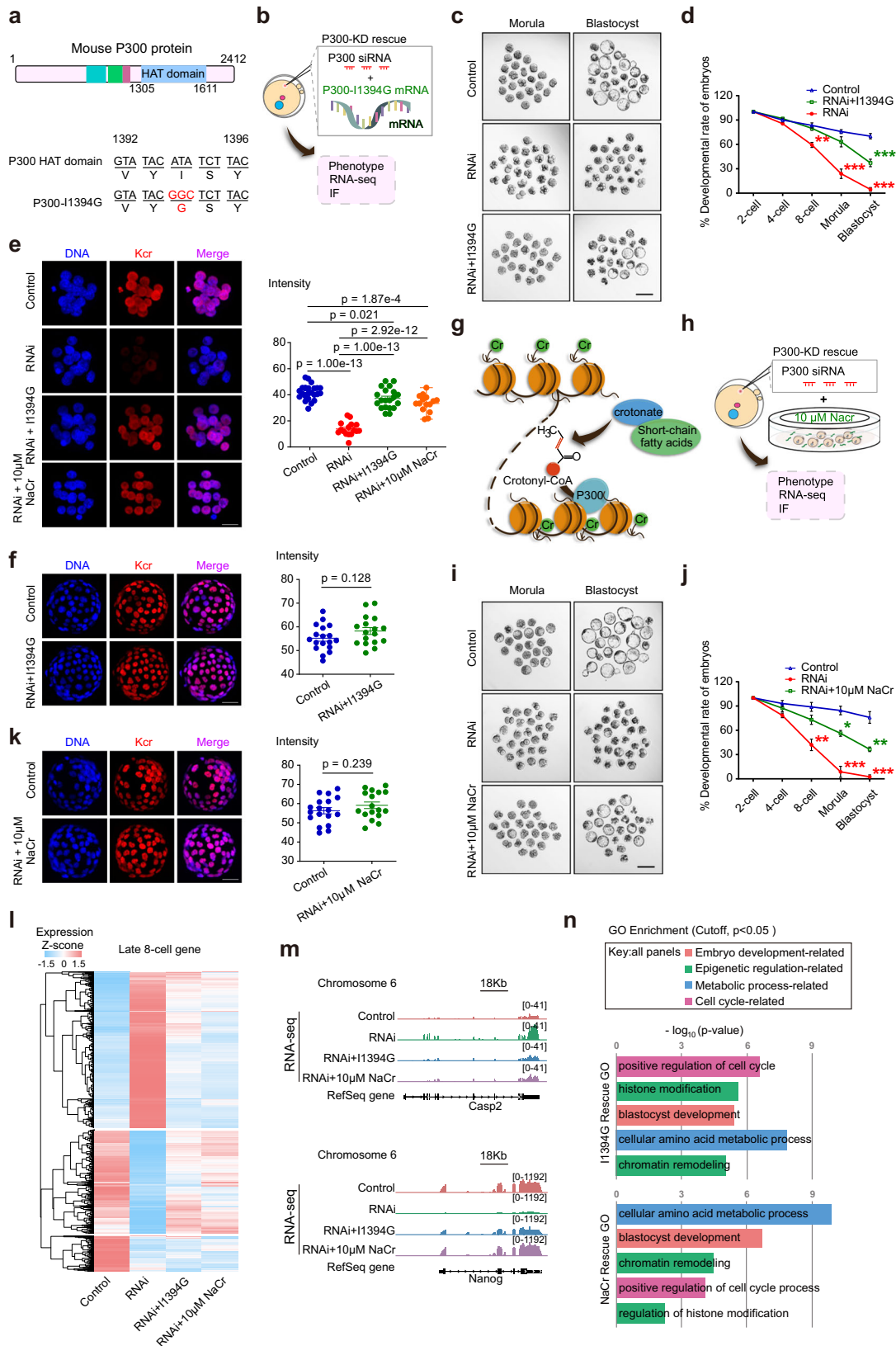
Fig. 4 | Effects of P300 knockdown on crotonylation of different lysine modification sites of histone H3 in the mouse preimplantation embryos.

a Representative image of immunofluorescence staining for crotonylation (Kcr) modification of lysine sites of histone H3 in late 8-cell stage embryos. Images are presented for both control and P300 knockdown (P300-KD) embryos. The experiment was conducted with three independent biological replicates, and similar results were obtained each time. Control ($n = 12$), P300-KD ($n = 15$). Scale bar: 20 μm . **b–h** Representative images of immunofluorescence staining for different lysine crotonylation (Kcr) modification of histone H3 in control and P300-KD embryos at late 8-cell stage, such as H3K18cr (**b**, Control $n = 15$, P300-KD $n = 15$), H3K9cr (**c**, Control $n = 23$, P300-KD $n = 20$), H3K23cr (**d**, Control $n = 20$, P300-KD

$n = 21$), H3K36cr (**e**, Control $n = 22$, P300-KD $n = 27$), H3K27cr (**f**, Control $n = 26$, P300-KD $n = 26$), H3K14cr (**g**, Control $n = 24$, P300-KD $n = 18$), and H4K12cr (**h**, Control $n = 25$, P300-KD $n = 29$). The experiment was conducted with three independent biological replicates, and similar results were obtained each time. Scale bar: 20 μm . **i** Immunofluorescence analyses of the crotonylation modification at different sites of histone H3 in late 8-cell embryos. Data are presented as mean values \pm SEM and were analyzed using two-tailed unpaired t -tests. **j** Western blot analysis of the histone lysine crotonylation (Kcr) modification at different lysine sites of H3 in control and P300 knockdown embryos. Each group consisted of 100 embryos, and a total of two independent biological replicates were conducted. α -Tubulin served as the control for normalization.

transcription. Next, we explored the connection between alterations in gene expression in the P300 knockdown embryos and the occupancy of H3K18cr. Cumulative distribution plots demonstrated a significant left-shift in the change of read coverage (FPKM) for H3K18cr target genes compared to non-target genes (Fig. 6g). Moreover, the cumulative distribution plots in the rescue groups were similar to those in

the control group (Fig. 6h, i). Representative track views further supported these findings, showing a significant reduction in transcriptional activities at the upstream and gene TSS regions in the P300 knockdown embryos at the late 8-cell stage (Fig. 6j). Similarly, the trend of H3K18cr and gene signal in the rescue group embryos were consistent with that in the control group, indicating a successful



rescue of gene transcription (Fig. 6j). Additionally, we also observed upregulated genes and conducted a comparative analysis of the modification intensity, peak number, and the relative position of H3K18cr between upregulated and downregulated genes. Our analysis revealed that the overall H3K18cr modification level at the TSS site was significantly higher in downregulated genes compared to upregulated

genes (Supplementary Fig. 12a). The peaks enriched in upregulated genes were slightly higher than those in downregulated genes (Supplementary Fig. 12b). Surprisingly, most of the H3K18cr modifications enriched in downregulated genes were distributed in the promoter regions of the genes, whereas the upregulated genes were mainly enriched in distal intergenic regions, with minimal enrichment at the

Fig. 5 | The rescue of P300 knockdown embryo development by P300-II394G mutant and crotonate. **a** Diagrams detail the mouse P300 gene structure and the specific mutation site in the P300-II394G mutant. **b** Schematic of the procedure for rescuing P300 knockdown embryos with the P300-II394G mutant. **c** Representative images of embryo development from the morula to blastocyst after P300-II394G rescue. RNAi: P300-KD. Control ($n = 82$), P300-KD ($n = 80$), P300-KD + II394G ($n = 78$). Scale bar: 100 μm . **d** Statistical analysis of the impact after rescue with P300-II394G mRNA on embryonic development rate ($n = 3$ biological replicates). Developmental stages: 8-cell ($P = 0.41$), Morula ($P = 0.13$), Blastocyst ($P = 5.99\text{e-}4$) for RNAi + II394G vs. control; 8-cell ($P = 1.20\text{e-}3$), Morula ($P = 3.70\text{e-}4$), Blastocyst ($P = 1.24\text{e-}5$) for RNAi vs. control. * $P < 0.05$; ** $P < 0.01$; *** $P < 0.001$. **e, f** Images show histone lysine crotonylation (Kcr) fluorescence in control, P300 knockdown, P300-II394G, and NaCr rescue embryos at the morula stage ($n = 23$, $n = 16$, $n = 20$, $n = 15$). At the blastocyst stage (control, $n = 18$, P300-II394G, $n = 17$). $n = 3$ biological replicates. Scale bar: 50 μm . **g** Representative images of key metabolic reactions involved in the generation of crotonyl-CoA. **h** Schematic of experimental procedure for rescuing P300 knockdown embryos by crotonate

(NaCr). **i** Representative images of embryo development from the morula to blastocyst after NaCr rescue. RNAi: P300-KD. Control ($n = 68$), P300-KD ($n = 75$), P300-KD + NaCr ($n = 71$). Scale bar: 100 μm . **j** Statistical analysis of the impact after rescue with NaCr on embryonic development rate ($n = 3$ biological replicates). Developmental stages: 8-cell ($P = 0.12$), Morula ($P = 0.01$), Blastocyst ($P = 0.001$) for RNAi + NaCr vs. control; 8-cell ($P = 1.67\text{e-}3$), Morula ($P = 6.15\text{e-}5$), Blastocyst ($P = 3.23\text{e-}5$) for RNAi vs. control. * $P < 0.05$; ** $P < 0.01$; *** $P < 0.001$. **k** Representative images of Kcr fluorescence in control, and NaCr rescue embryos at blastocyst ($n = 18$, $n = 17$) stage. $n = 3$ biological replicates. Scale bar: 50 μm . **l** Heatmap showing differential gene expression after rescue at the late 8-cell stage. **m** Track views display the enrichment of RNA-seq signals in control, P300 knockdown, and P300-II394G or NaCr rescue embryos. **n** GO enrichment analysis was conducted to evaluate the rescued genes after P300-II394G and NaCr rescue. In **(d)**, **(e)**, **(f)**, **(j)**, and **(k)**, data are presented as mean values \pm SEM. In **(d)**, **(e)**, and **(j)**, statistical analysis was subjected to one-way ANOVA for analysis. In **(f)** and **(k)**, was performed using two-tailed unpaired t -tests.

TSS site (Supplementary Fig. 12c). Altogether, these results suggest that H3K18cr may serve as a key marker and contribute to the activity of gene transcription.

During embryonic development, gene expression is facilitated by the enlistment of Pol II at target gene promoters, a process orchestrated by general transcription factors that recognize specific DNA sequence motifs^{7,29}. This conclusion suggests that Pol II binding is positively correlated with gene expression. To investigate the correlation between Pol II and H3K18cr occupancy after P300 knockdown, we classified them into three types based on the comparison between P300 knockdown and control: upregulated, downregulated, and unchanged (Fig. 7a). The analysis of the upregulated H3K18cr peaks after P300 knockdown revealed a significant increase in Pol II enrichment signal in the P300 knockdown embryos (Fig. 7b). Conversely, the downregulated H3K18cr peaks showed a significant reduction in the Pol II enrichment signal in the P300 knockdown embryos (Fig. 7c). The unchanged H3K18cr peaks exhibited no noticeable differences between the P300 knockdown and the control groups (Fig. 7d). Supporting these results, a representative track view demonstrated increased Pol II peaks along the *Ccng1* gene from the TSS to the TES regions in the P300 knockdown embryos. In contrast, the track view of the *Myc* gene showed significantly reduced Pol II peaks in the P300 knockdown embryos, while the Pol II peaks of the *Kdm5b* gene remained unchanged (Fig. 7e).

Following ZGA, canonical H3K4me3 is established at the promoter regions, while most transcriptional repressive markers are removed from the promoter regions, indicating that H3K4me3 could serve as a potential hallmark of transcriptional activation^{30,31}. Accordingly, we further investigated the alterations in H3K4me3 modification levels after P300 knockdown. The results revealed a significant decrease in H3K4me3 signals at the transcription start site (TSS) region (Supplementary Fig. 12d). Importantly, our previous findings indicated a reduction in H3K18cr signals in the TSS region after P300 knockdown (Fig. 6e), suggesting a potential synergistic effect between H3K18cr and H3K4me3 modifications. Subsequently, we conducted a correlation analysis between H3K18cr and H3K4me3 occupancy following P300 knockdown (Supplementary Fig. 12e). In the analysis of the upregulated H3K18cr peaks after P300 knockdown, there was a significant increase in H3K4me3 enrichment signal specifically at the TSS regions after P300 knockdown (Supplementary Fig. 12e, f). Correspondingly, the downregulated H3K18cr peaks showed a significant decrease in the H3K4me3 enrichment signal at the TSS regions (Supplementary Fig. 12e, g). The unchanged H3K18cr peaks exhibited no significant difference in the H3K4me3 signal at the TSS regions between the P300 knockdown group and the control group (Supplementary Fig. 12e, h). In addition, we observed an overlap between the number of 6712 (58.20%) upregulated and 2643 (84.82%)

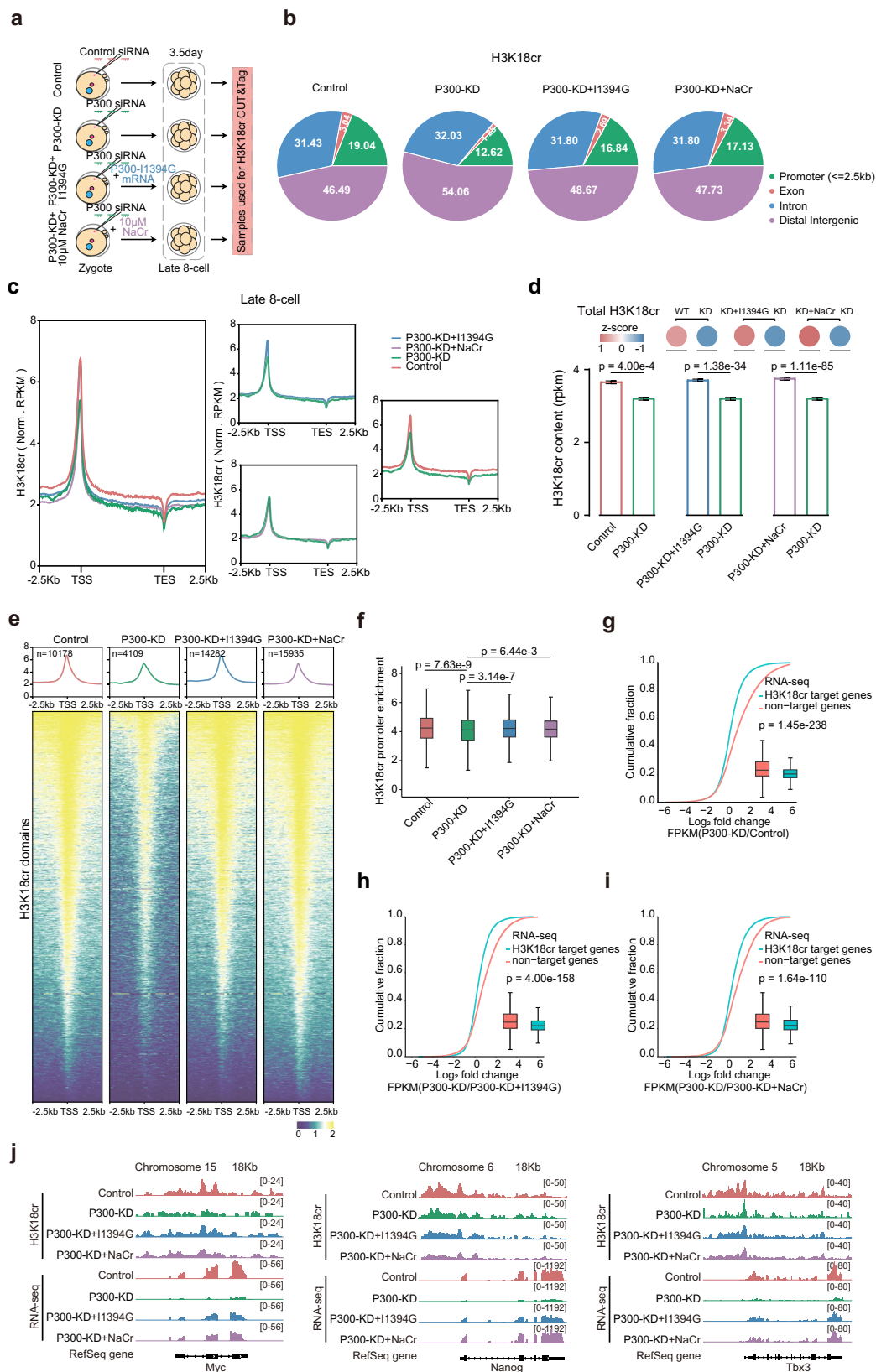
downregulated genes in both modifications, while some genes are regulated by only one type of modification (Supplementary Fig. 12i). Among the genes regulated by H3K4me3 modification, 2538 genes were upregulated, whereas 10799 genes were downregulated. Similarly, among those regulated by H3K18cr modification, 4820 genes were upregulated, while 473 genes were downregulated (Supplementary Fig. 12i). Therefore, our research findings suggest that H3K18cr and H3K4me3 may co-localize at some active genes and exhibit partial synergistic effects. However, there are also some genes specifically regulated by either H3K18cr or H3K4me3.

Overall, our findings support the notion that H3K18cr plays a positive regulatory role in gene transcription during preimplantation embryonic development. The observed changes in the H3K18cr levels, particularly at the TSS regions, upon P300 knockdown may contribute to transcriptional dysregulation and the developmental defects observed in these embryos. Collectively, these findings confirm that H3K18cr positively regulates gene transcription to promote preimplantation embryonic development.

Discussion

Although previous studies have shown that histone crotonylation localizes to potential enhancer and promoter regions of active genes in the mammalian genome^{13,16}, the distribution and function of histone crotonylation during preimplantation embryo development remain unknown. In this study, we provided functional evidence that P300-mediated histone crotonylation modifications are essential for preimplantation embryo development. Depletion of the P300 transcripts leads to embryonic developmental arrest and defects and dysregulation of the transcriptome. Specifically, we found that a significant reduction in histone crotonylation, particularly H3K18cr, is responsible for embryo developmental arrest. Furthermore, we delved into the potential roles of histone crotonylation as a pivotal regulatory mechanism governing gene transcription and preimplantation embryo development fate. Under normal conditions, the transcriptional coactivator P300 mediates crotonylation of histone and maintains a high level, regulating the normal transcription of genes, thereby ensuring a successful transition of embryos from the 8-cell to morula stage, and subsequently leading to the development of blastocysts. On the other hand, abnormal crotonylation leads to dysregulation of gene expression, resulting in embryo arrest at the 8-cell stage and fragmentation, with retention of 8-cell-like morphological characteristics (Fig. 7f). This study provides the first insights into the roles and molecular mechanisms of histone crotonylation during preimplantation embryo development.

Transcription factors act as pioneering elements responsible for the recruitment of Pol II³². Subsequently, Pol II undergoes a pre-configuration process, ensuring precise coordination between



chromatin maturation and initiation of the genomic clock⁷. P300 is a transcriptional coactivator for many important transcription factors, mediating the binding of transcription factors and Pol II^{26,33}. Studies have shown that P300 is a highly translated maternal factor in zebrafish that acts as a temporal switch, conferring transcriptional

competency and regulating the timing and output of transcription during ZGA³⁴. Our results suggest that P300 is an important regulatory factor that initiates transcription and translation in mouse early embryonic development (Fig. 1a–d). The knockdown of P300 altered the normal gene expression patterns (Fig. 2c, d), resulting in impaired

Fig. 6 | Correlation analysis between P300-mediated H3K18cr modification and transcripts. **a** Schematic of sample collection for H3K18cr CUT&Tag analysis in control, P300 knockdown (P300-KD), and P300-I1394G or NaCr rescue embryos. **b** Pie chart showing the distribution of H3K18cr peaks across annotated genomic regions in control, P300-KD, P300-I1394G rescue, and NaCr rescue embryos at late 8-cell stages. **c** Enrichment profiles show the fluctuation of H3K18cr signals in control, P300-KD, P300-I1394G rescue, and NaCr rescue embryos at late 8-cell stages. **d** Combination Column and Bubble Charts show the difference in total H3K18cr modification peaks ($n = 25209$) among control, P300-KD, P300-I1394G rescue, and NaCr rescue embryos at the late 8-cell stages. Data are presented as mean values \pm SEM. $n = 2$ biological replicates. Statistical analysis was performed using two-tailed unpaired *t*-tests. **e** Comparison of the occupancy of H3K18cr around the TSS region ($TSS \pm 2.5$ kb) in control, P300-KD, and P300-I1394G or NaCr rescue embryos. **f** Boxplots showing the signals of the H3K18cr promoter region (two biological replicates) at global genes of different experiment groups. Control

($n = 7934$), P300-KD ($n = 3674$), P300-KD + I1394G ($n = 10175$), P300-KD + NaCr ($n = 11181$). **g–i** The plot displays the cumulative frequency of \log_2 fold changes in FPKM among control (**g**, target $n = 7553$, non-target $n = 9690$), P300-I1394G rescue (**h**, target $n = 9697$, non-target $n = 8037$), NaCr rescue (**i**, target $n = 10448$, non-target $n = 6667$), and P300 knockdown embryos. A noticeable shift to the left for H3K18cr target genes suggests an overall positive alteration in gene expression. $n = 2$ biological replicates. **j** Track views display the enrichment of H3K18cr peaks and RNA-seq signals among control, P300-KD, and P300-I1394G or NaCr rescue embryos. The vertical axis corresponds to normalized tag counts for H3K18cr peaks and RNA-seq in each sample. Refgene refers to the genome data from NCBI and IGV. In (**d**), (**f**), (**g**), (**h**), and (**i**), Statistical analysis was performed using two-tailed unpaired *t*-tests. The center line and edges of the boxes represent the median and quartiles of the data points, respectively. The minimum and maximum values in the boxplots correspond to quartile 1 $- 1.5 \times$ interquartile range and quartile 3 $+ 1.5 \times$ interquartile range, respectively.

embryo developmental competence and poor embryonic quality (Fig. 1e–h). Moreover, we observed that the knockdown of P300 significantly affected Pol II enrichment at gene body regions of the embryonic genome (Fig. 3f–h), leading to aberrant transcriptional elongation. This discovery aligns with a recent investigation indicating that P300 stabilizes Pol II and promotes Pol II pausing³⁵. H3K4me3 is a well-established indicator of active promoter, facilitating the recruitment of chromatin remodelers and transcriptional regulators^{30,31,36}. When early embryos undergo major ZGA, classical H3K4me3 replaces the non-classical H3K4me3 (ncH3K4me3) enriched in the promoter regions^{31,36}. This transition renders H3K4me3 a distinct and intimately associated marker for transcriptional regulation in early embryos. Our finding shows that knockdown of P300 significantly altered H3K4me3 enrichment at TSS regions of the embryonic genome (Supplementary Fig. 12e). Remarkably, the distinct peaks of H3K18cr and H3K4me3 after P300 knockdown exhibited a parallel trend at the TSS, indicating a potential synergistic interplay between H3K18cr and H3K4me3 during early embryo development (Supplementary Fig. 12e–h). Briefly, our results displayed that P300 is required for early embryonic development and highlight a positive correlation between Pol II, H3K4me3, and transcriptome changes after P300 knockdown.

Lysine histone crotonylation is one of the histone lysine acylation modifications, occurring on the ϵ -amino group of lysine residues in histone side chains. This modification leads to the neutralization of the positive charge of these residues^{13,37}. The reduction in positive charge on the histone lysine residues results in a weakened interaction with DNA, leading to a more relaxed chromatin structure that becomes more accessible to DNA-binding factors. The presence of crotonylation has been verified in various microorganisms, plants, and animals through mass spectrometry and proteomics^{18,38,39}. In previous studies, histone lysine crotonylation, as an indicator of gene expression, has been implicated in the regulation of gene transcription. For instance, in male germ cells following meiosis, histone crotonylation becomes enriched on sex chromosomes, particularly marking a subset of genes specific to the testis. Within this context, the chromodomain Y-like transcription corepressor (CDYL) exerts a negative regulatory role on histone crotonylation, ultimately leading to the repression of transcription^{22,40}. In the female germ cells, the increased levels of histone crotonylation lead to enhanced expression of endothelial genes during the differentiation of human embryonic stem cells¹⁶. Our study revealed dynamic changes in histone crotonylation during implantation embryo development (Supplementary Fig. 6d), suggesting a critical role for histone crotonylation in embryonic development. Previous studies have demonstrated that P300 mutants with competent HCT activity were able to enhance transcriptional activation¹⁹. In our study, immunofluorescence and RNA-seq data showed a significant reduction in histone crotonylation levels upon P300 knockdown (Fig. 4), accompanied by notable changes in the transcriptome (Fig. 2c, d). Remarkably, in the embryos rescued by the P300 mutant,

the levels of these abnormally elevated transcripts were largely restored, while the downregulated transcripts exhibited partial recovery to normal expression levels (Fig. 5l) after rescue. These results suggest that histone crotonylation is involved in the regulation of gene transcription during embryonic development. Additionally, metabolism also plays a critical role in cell-fate decisions through epigenetic regulation^{15,41}. The conversion of the short-chain fatty acid (SCFA) crotonate into crotonyl-CoA, results in increased histone crotonylation levels in cellular metabolism¹⁴. Our results demonstrated that the embryo developmental rates and transcription levels of genes were remarkably restored in the crotonate rescue group (Fig. 5i–l). These findings suggest that histone crotonylation does regulate early embryonic development and the transcription of genes.

Several factors are involved in the regulation of histone crotonylation-mediated gene expression. These factors act as writers, erasers, and readers of histone crotonylation marks. P300 is the major HCT in mammalian cells^{19,42}. We observed a global decrease in crotonylation levels in the P300 knockdown embryos, particularly with a significant reduction in the crotonylation modification of lysine 18 on histone H3. (Fig. 4b, i). However, the knockdown of P300 not only affected the H3K18cr levels but also led to diverse changes in histone crotonylation at other sites during preimplantation embryo development (Fig. 4c–i). The variance in the identification of P300 substrates during early embryogenesis may arise from distinctions in species and cell types. The potential impact of P300 inhibition on alternate substrates cannot be excluded, particularly considering P300 also catalyzes the modification of non-histone proteins in some cell types⁴³. Consequently, further investigations are warranted to address this aspect in future studies.

Various histone crotonylation sites have been associated with active chromatin and gene activation¹⁴. Our data revealed enrichment of H3K18cr peaks at promoters, introns, and distal regions in preimplantation embryos (Supplementary Fig. 10a, b). Importantly, we observed a significant reduction in the H3K18cr signal at TSS regions following P300 knockdown (Fig. 6e, f), suggesting a potential role for H3K18cr in gene transcription regulation. Furthermore, the changed peaks of H3K18cr enrichment correlated positively with changes in the transcriptome, Pol II, and H3K4me3 occupancy after P300 knockdown, as observed through CUT&Tag and RNA-seq data (Figs. 3f, 6e and Supplementary Fig. 12e–h). These results imply that H3K18cr positively regulates gene transcription during embryonic development. Consistent with our findings, CDYL, a chromodomain-containing protein, has been shown to regulate histone crotonylation negatively. Overexpression of CDYL leads to diminished H3K18cr levels in the majority of its target genes, and the magnitude of H3K18cr reduction mediated by CDYL correlates with the broader suppression of global histone crotonylation^{22,44}. Additionally, histone deacetylation is mediated by members of the class I histone deacetylase family, including HDAC1, HDAC2, and HDAC3²³. Deletion of HDAC1/2 has been

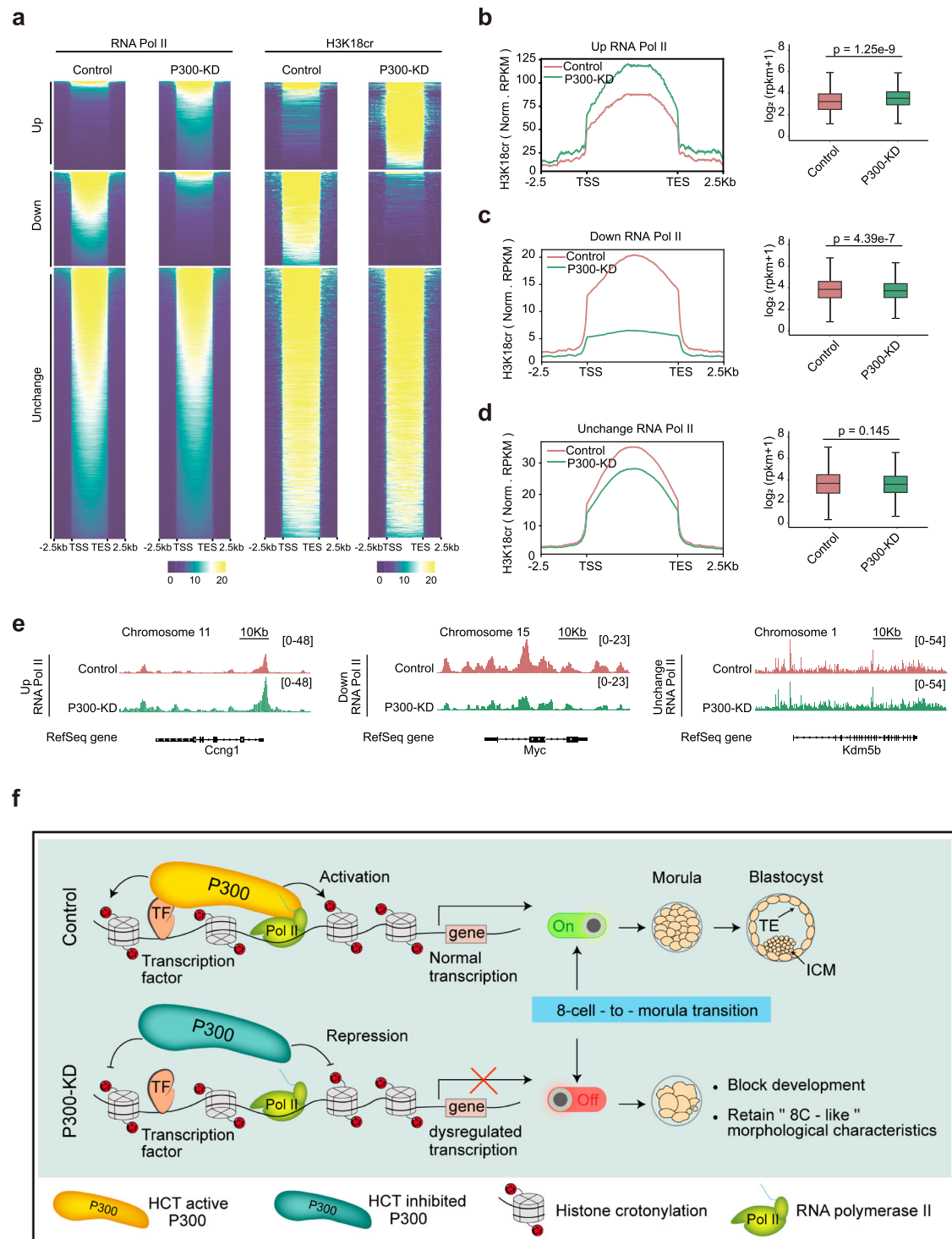


Fig. 7 | Correlation analysis between P300-mediated H3K18cr modification and RNA-Pol II. **a** Heatmaps showing the differentially H3K18cr peaks and their gene body RNA-Pol II enrichment in control and P300 knockdown (P300-KD) embryos. TSS, transcription start site. TES, transcription end site. **b–d** The average plot showing the differentially H3K18cr peaks led to global changes of RNA Pol II enrichment at the gene body regions, such as upregulated (**b**, Control $n = 768$, P300-KD $n = 786$), downregulated (**c**, Control $n = 2108$, P300-KD $n = 1848$), and unchanged (**d**, Control $n = 2843$, P300-KD $n = 2628$). Statistical analysis was performed using two-tailed unpaired t -tests. The center line and edges of the boxes represent the median and quartiles of the data points, respectively. The minimum and maximum values in the boxplots correspond to quartile 1–1.5 \times interquartile range and quartile 3 + 1.5 \times interquartile range, respectively. $n = 2$ biological replicates. **e** Representative tracks show occupancy of RNA-Pol II at the gene body

regions of genes (*Ccng1*, *Myc*, and *Kdm5b*) in the control and P300 knockdown embryos (two biological replicates). **f** Working model illustrating how P300-mediated histone crotonylation regulates the preimplantation embryo development. P300-mediated histone crotonylation plays a pivotal role in preimplantation embryo development. Under normal conditions, P300 facilitates the crotonylation modification of histones, maintaining a high level of this modification. As a result, genes are transcribed appropriately, ensuring successful embryo development from the 8-cell to the morula stage, and further maturation into the blastocyst. On the other hand, when P300 expression is depleted, the level of crotonylation becomes abnormal, which leads to dysregulated gene expression, disrupting the delicate balance required for proper development. Consequently, the embryos are arrested at the 8-cell stage and exhibit fragmented structures, retaining characteristics similar to 8-cell embryos.

shown to lead to a significant enrichment of H3K18cr at genes in embryonic stem cells (ESCs), particularly in genes involved in embryonic morphogenesis and development⁴⁵. All of the above results collectively support the positive correlation between H3K18cr modification and gene transcription regulation. In summary, our results demonstrate that P300 acts as a key regulatory factor positively regulating H3K18cr to promote preimplantation embryonic development. However, further investigations are warranted to determine the genome-wide distribution of H3K18cr at different stages of early embryo development and the specific role of H3K18cr in modulating developmental events during mammalian embryogenesis.

In conclusion, our study highlights the essential role of P300 as a histone crotonyltransferase in early embryonic development. The specific enrichment of H3K18cr at promoter regions promotes genome-wide transcription activation and proper gene expression, which is crucial for embryonic development. These findings further enhance our understanding of the epigenetic regulation of early embryo development.

Methods

The animal use protocol listed below has been reviewed and approved by the Animal Ethics Committee of Guangdong Second Provincial General Hospital. Approval number: 2022-DW-KZ-011-02. Moreover, unless stated otherwise, all chemicals were procured from Sigma (Sigma-Aldrich, St. Louis, MO).

Mouse embryo collection and in vitro culture

Experimental mice were housed within the controlled confines of the Guangdong Second Provincial General Hospital, maintaining a temperature range of 22–25 °C, relative humidity at 60%, and a 12-h light/dark cycle. These mice had unrestricted access to water and food. Super-ovulation of 8-week-old female BDF1 (C57BL/6 × DBA/2) mice was achieved through intraperitoneal administration of 7.5 IU PMSG, followed by injection of 7.5 IU hCG after 48 h. These females were then paired with BDF1 male mice for mating. After an 18-h period, mice were humanely euthanized, and zygotes were carefully harvested from the expanded upper oviduct. The encompassing cumulus cells were gently eliminated using a 0.03 mg/ml hyaluronidase solution. Pools of 20 zygotes were cultured in 50 µl droplets of KSOM (Millipore, MR-107-D) at 37 °C, in an environment consisting of 5% CO₂ in air and optimal humidity.

Microinjection

P300 siRNA sequences were meticulously designed to target distinct regions within mouse *P300* mRNA. Microinjection procedures were conducted in the M2 medium. Around 10 µl of siRNA solution (30 µM) or mRNA (500 ng/µl) was meticulously microinjected into the cytoplasm of zygotes or 2-cell blastomeres, with the manipulated samples subsequently undergoing incubation in KSOM. The negative control siRNA was introduced as the control counterpart, thereby enabling the assessment of potential microinjection impacts. The negative control siRNA oligo (sense sequence: 5'-UUCUCCGAACGUGUCACGUTT-3'; antisense sequence: 5'-ACGUGACACGUUCGGAGAATT-3'; GenePharma, Shanghai, China), P300-mus-4127 (sense sequence: 5'-GCAU GCAUGUUAAGAAUATT-3'; antisense sequence: 5'-UAUUCUUGAA-CAUGCAUGCTT-3'; GenePharma, Shanghai, China), P300-mus-4346 (sense sequence: 5'-GCCAUCCACCUGAUCAGAATT-3'; antisense sequence: 5'-UUCUGAUCAGGUGGAUGGCTT-3'; GenePharma, Shanghai, China).

Cell culture and transfection

Murine embryonic fibroblast (MEF) cells were derived from 13.5-day embryos and cultured in the Dulbecco's modified Eagle's medium (DMEM, Gibco, 11995065) supplemented with 10% fetal bovine serum (FBS, Gibco, 10099141C), penicillin/streptomycin (Pen Strep, Gibco,

15140-122), and were maintained at 37 °C in 5% CO₂ in air. The mouse embryonic stem cell (mESC) lines used were E14. These cells were cultured in feeder-free conditions on gelatin-coated culture dishes (0.1% gelatin, Beyotime, C0316). mESCs were maintained in Knockout DMEM supplemented with 15% FBS, 2 mM GlutaMAX (Gibco, 35050061), 100 U/ml penicillin/streptomycin (Pen Strep, Gibco, 15140-122), 0.1 mM β-mercaptoethanol, 0.1 mM Non-Essential Amino Acids (NEAA, Gibco, 11140050), 1 µM PD0325901 (LC Laboratories, P-9688), 1000 U/ml leukemia inhibitory factor (LIF, Millipore, ESG1107), 3 µM CHIR99021 (LC Laboratories, C-6556). Following the manufacturer's instructions, Lipofectamine 3000 Transfection Reagent (Thermo Fisher, L3000015) was utilized for the transfection of cells.

Quantitative polymerase chain reaction (qPCR)

Pools of 20 zygotes or embryos at different developmental stages were collected, and total RNA was extracted using the RNeasy Micro Kit (Qiagen, 34004) following the manufacturer's instructions. Reverse transcription was performed with the QuantiTect Reverse Transcription Kit (Qiagen, 205311). Quantitative PCR was carried out using the SYBR Green PCR Master Mix (Qiagen, 208054) according to the manufacturer's protocol on The LightCycler® 480 Instrument II System. For the gene expression analysis, the 2^{-ΔΔCT} method was employed for relative quantification, utilizing H2afz as the internal reference gene. All experimental procedures were independently replicated three times using distinct biological samples. The primer sequences utilized for these assays can be found in Supplementary information.

Immunofluorescence staining

At room temperature, embryos were fixed in 4% paraformaldehyde (PFA) for 30 min, followed by permeabilization with 0.5% Triton X-100 for 30 min. The samples were blocked with PBS containing 10% FBS for 1 h. Subsequently, embryos were sequentially incubated with primary and secondary antibodies. After washing again with PBS + 0.1% PVP, the embryos were stained with DAPI for 10 min. Subsequently, they were mounted onto glass slides and covered using glass coverslips. The specific experimental steps were referenced from the previous protocol⁴⁶. Confocal fluorescence microscopy (Olympus, Tokyo, Japan) was used for imaging the samples. All images were captured without adjusting contrast or brightness, and the same parameters were used for photography. Quantitative analysis of fluorescence signal intensity and cell counting was conducted using the Image J software (NIH, Bethesda, MD, USA; version 1.52a). All nuclei from each embryo were counted, and the average value was calculated as the fluorescence intensity value of the embryo. The primary antibodies used are listed in Supplementary information.

EU incorporation assay

The embryos at different developmental stages were acquired and cultured in KSOM medium supplemented with 500 µM 5-ethynyluridine (EU) for 2 h at 37 °C with 5% CO₂ in a saturated humidity environment. After the incubation, at room temperature, embryos were fixed in 4% paraformaldehyde (PFA) for 30 min, followed by permeabilization with 0.5% Triton X-100 for 30 min. To detect the incorporated EU, the Cell-Light EU Apollo 488 In vitro Imaging Kit (RiboBio, C10316-3) was used, following the manufacturer's protocol. After the detection process, the samples were imaged using a confocal fluorescence microscope to visualize and analyze the distribution of EU-labeled transcripts.

Western blotting

The Western blotting experiment was conducted following our previously established research protocol with minor modifications⁴⁶. Embryos were collected and placed in lysis buffer containing protein sample buffer (Beyotime, P0012B), followed by boiling at 95 °C for 10 min. Protein samples were separated using sodium dodecyl sulfate-

polyacrylamide gel electrophoresis (Mini-PROTEAN Tetra, Bio-Rad, Berkeley, CA, USA). Following separation, proteins were transferred onto membranes using an electrophoretic transfer apparatus (Trans-Blot, Bio-Rad, Berkeley, CA, USA). The subsequent steps involved incubation with primary and secondary antibodies, and the resulting images were captured using the VersaDoc imaging system (3000, Bio-Rad, Berkeley, CA, USA). Supplementary information contains detailed information about the primary and secondary antibodies utilized in this research.

Preparation of recombinant I1394G mutant

T7-driven vectors were utilized to subclone mutant cDNA for P300. The construction of the P300 mutant (I1394G) followed previously established methods¹⁹. All sequences underwent validation through Sanger sequencing by GENEWIZ (GENEWIZ, Guangzhou, China) prior to their application. According to the manufacturer's manual to prepare mRNA, plasmids were linearized and subjected to *in vitro* transcription, capping, and poly (A) tailing using the T7 Mmessage mMACHINE Kit (Thermo Fisher Scientific, AM1344). Subsequent purification and recovery of RNA were accomplished using the RNA Clean Beads (Vazyme, N412-02).

RNA-seq library generation and sequencing

The Smart-seq2 protocol was employed to create total RNA-seq libraries from early embryos at various developmental stages⁴⁷. In brief, embryos at 4-cell, early 8-cell, and late 8-cell stages, visually confirmed under a microscope, were lysed in lysis buffer supplemented with RNase inhibitor (RiboLock RNase, Thermo Fisher Scientific, EO0382), 10 mM dNTP mix (NEB, Cat#N0447), and polyadenylated mRNAs were isolated using the oligo-dT primer (5'-AACGACAGACT30VN-3'). After a 5-min lysis step at 72 °C, reverse transcription of RNAs was carried out using random hexamers, followed by PCR amplification. Subsequently, cDNAs were pre-amplified, purified using Ampure XP beads (Beckman Coulter, Brea, California, USA), and subjected to tagmentation using the Tn5 transposase. The Illumina TruSeq library preparation was then performed. The sequencing of all libraries was conducted on the Illumina HiSeq 6000 sequencers. Each sample was subjected to two independent biological replicates.

CUT&Tag library generation and sequencing

The CUT&Tag library protocol was adapted from a previous study with slight modifications⁴⁸. In summary, MEF cells, late 8-cell embryos, and morula stage embryos were gently washed with 100 μ l of wash buffer (20 mM HEPES (pH 7.5); 150 mM NaCl; 0.5 mM Spermidine; 1x Protease inhibitor cocktail). Subsequently, the samples were incubated with 10 μ l of activated Concanavalin A coated magnetic beads (ConA beads, Vazyme) for 15 min at room temperature. After discarding the unbound supernatant, the bead-bound cells were resuspended in 50 μ l of antibody buffer (20 mM HEPES (pH 7.5); 150 mM NaCl; 0.5 mM Spermidine; 1x Protease inhibitor cocktail; 0.05% Digitonin; 2 mM EDTA) containing the appropriate primary antibody and incubated overnight at 4 °C. The primary antibody was removed by magnetic separation. Following two washes with the dig-wash buffer (20 mM HEPES (pH 7.5); 150 mM NaCl; 0.5 mM Spermidine; 1x Protease inhibitor cocktail; 0.05% Digitonin), the secondary antibody (diluted 1:50 in 50 μ l of dig-wash buffer) was applied for 1 h at room temperature. Cells were washed twice with the dig-wash buffer to eliminate unbound antibodies using magnetic separation. Next, the Tn5-protein A/G adapter complex (0.04 μ M) was prepared in the dig-300 buffer (20 mM HEPES (pH 7.5); 300 mM NaCl; 0.5 mM Spermidine; 1x Protease inhibitor cocktail; 0.05% Digitonin), and the samples were incubated for 2 h at room temperature. After washing the samples twice with the dig-300 buffer, the samples were resuspended in 25 μ l of tagmentation buffer and incubated at 37 °C for 2 h. Subsequently,

tagmentation was halted at 55 °C using 10% SDS for 15 min. DNA extraction was performed using activated DNA Extract Beads. The DNA of the sample was mixed with different index primers to amplify libraries. Next, the libraries were subjected to Ampure XP beads (Beckman Coulter) and 80% ethanol purification. The Illumina HiSeq 3000 or 4000 sequencers were used for the sequencing of all libraries.

Data analyses

Gene expression data processing. Utilizing Tophat (version 2.4.0)⁴⁹, the RNA-seq data were aligned to the mm9 genome. Subsequently, the gene expression levels were computed using Cufflinks (version 2.2.1)⁴⁹, with reference to the mm9 refFlat annotation database from the IGV browser.

RNA-seq data mapping. Conducting biological replicates for each sample, RNA-seq analysis was executed. Raw reads underwent trimming using Cutadapt version 4.1⁵⁰ and were subsequently mapped to the mouse genome (mm9) utilizing Hisat2 version 2.2.1⁵¹ with default parameters. Uniquely mapped reads were subsequently assembled into transcripts guided by reference annotation (the University of California Santa Cruz [UCSC] gene models) using Cufflinks version 2.2⁴⁹. Gene expression levels were quantified as FPKM. Functional annotation was conducted through clusterprofiler (V4.0)⁵². Statistical analyses were carried out using the R software (<http://www.rproject.org>). Calculation of Spearman correlation coefficient (rs) utilized the cor function, and gene clustering employed the complete linkage hierarchical algorithm. Quality controls for the RNA-seq results are detailed in the Extended materials.

CUT&Tag data analysis. The mouse genome (UCSC mm9) served as the reference for aligning all paired-end CUT&Tag reads, performed using Bowtie2 version 2.3.5.1 with default parameters. Only uniquely mapping reads with a tolerance of up to two mismatches were retained⁵³. For subsequent analyses, read counts were normalized by calculating reads per kilobase of bin per million of sequenced reads (RPKM), following the removal of non-uniquely mapped reads, unmapped reads, and PCR duplicates. The track files were generated using the bamCoverage command from deepTools version 3.5.1⁵⁴. Identification of CUT&Tag peaks was carried out employing MACS (model-based analysis of ChIP-seq) version 2.1.2, using default parameters and a q-value cutoff of 0.05⁵⁵. Annotation of the distribution of CUT&Tag peaks was achieved through the utilization of the R package ChIPseeker⁵⁶. For the specified windows, heatmaps, metaplots, and metagene plots were generated, utilizing the average coverage (RPKM).

Data statistical analysis. In order to ensure the reliability of the experimental results, all the aforementioned experiments were conducted with multiple biological replicates. Statistical analysis of the collected data was performed using the SPSS software (version 17.0, SPSS, <https://spss.software.informer.com/17.0/>). Statistical analysis included the utilization of the independent-sample Student's *t*-test to evaluate distinctions between two groups, whereas, for the analysis of multiple groups, one-way ANOVA was applied, followed by subsequent multiple comparison tests. Statistically significant results are denoted by asterisks (**P* < 0.05), (***P* < 0.01), and (***)*P* < 0.001, respectively.

Reporting summary

Further information on research design is available in the Nature Portfolio Reporting Summary linked to this article.

Data availability

All data have been deposited to GEO with the accession number GSE241196. Publicly available datasets used in this work were from NCBI GEO accession number GSE45719 (RNA-seq data), <https://doi.org/10.1038/s41467-024-50731-0>

[org/10.1126/science.1245316](https://doi.org/10.1126/science.1245316); GSE135457 (Pol II Stacc-seq data), <https://doi.org/10.1038/s41586-020-2847-y>; GSE207222 (H3K27ac CUT&RUN data), <https://doi.org/10.15252/embj.2022112012>. Source data are provided with this paper.

Code availability

This study did not make any custom code or algorithm. All software used in this study are publicly available and cited in the main text and/or “Methods” section.

References

- Xu, R., Li, C., Liu, X. & Gao, S. Insights into epigenetic patterns in mammalian early embryos. *Protein Cell* **12**, 7–28 (2021).
- Xu, Q. & Xie, W. Epigenome in early mammalian development: inheritance, reprogramming and establishment. *Trends Cell Biol.* **28**, 237–253 (2018).
- Du, Z., Zhang, K. & Xie, W. Epigenetic reprogramming in early animal development. *Cold Spring Harb. Perspect. Biol.* **14**, a039677 (2022).
- Fu, X., Zhang, C. & Zhang, Y. Epigenetic regulation of mouse preimplantation embryo development. *Curr. Opin. Genet. Dev.* **64**, 13–20 (2020).
- Li, X., Egervari, G., Wang, Y., Berger, S. L. & Lu, Z. Regulation of chromatin and gene expression by metabolic enzymes and metabolites. *Nat. Rev. Mol. Cell Biol.* **19**, 563–578 (2018).
- Abuhashem, A. et al. RNA Pol II pausing facilitates phased pluripotency transitions by buffering transcription. *Genes Dev.* **36**, 770–789 (2022).
- Liu, B. et al. The landscape of RNA Pol II binding reveals a stepwise transition during ZGA. *Nature* **587**, 139–144 (2020).
- Wang, H. et al. H3K4me3 regulates RNA polymerase II promoter-proximal pause-release. *Nature* **615**, 339–348 (2023).
- Zhang, Y. et al. Dynamic epigenomic landscapes during early lineage specification in mouse embryos. *Nat. Genet.* **50**, 96–105 (2018).
- Chen, Z., Djekidel, M. N. & Zhang, Y. Distinct dynamics and functions of H2AK119ub1 and H3K27me3 in mouse preimplantation embryos. *Nat. Genet.* **53**, 551–563 (2021).
- Zhao, S., Zhang, X. & Li, H. Beyond histone acetylation-writing and erasing histone acylations. *Curr. Opin. Struct. Biol.* **53**, 169–177 (2018).
- Zhang, D. et al. Metabolic regulation of gene expression by histone lactylation. *Nature* **574**, 575–580 (2019).
- Tan, M. et al. Identification of 67 histone marks and histone lysine crotonylation as a new type of histone modification. *Cell* **146**, 1016–1028 (2011).
- Sabari, B. R. et al. Intracellular crotonyl-CoA stimulates transcription through p300-catalyzed histone crotonylation. *Mol. Cell* **58**, 203–215 (2015).
- Sabari, B. R., Zhang, D., Allis, C. D. & Zhao, Y. Metabolic regulation of gene expression through histone acylations. *Nat. Rev. Mol. Cell Biol.* **18**, 90–101 (2017).
- Fang, Y. et al. Histone crotonylation promotes mesoendodermal commitment of human embryonic stem cells. *Cell Stem Cell* **28**, 748–763.e747 (2021).
- Xiao, Y. et al. HBO1 is a versatile histone acyltransferase critical for promoter histone acylations. *Nucleic Acids Res.* **49**, 8037–8059 (2021).
- Lu, Y. et al. Dynamics and functional interplay of histone lysine butyrylation, crotonylation, and acetylation in rice under starvation and submergence. *Genome Biol.* **19**, 144 (2018).
- Liu, X. et al. MOF as an evolutionarily conserved histone crotonyltransferase and transcriptional activation by histone acetyltransferase-deficient and crotonyltransferase-competent CBP/p300. *Cell Discov.* **3**, 17016 (2017).
- Kaczmarek, Z. et al. Structure of p300 in complex with acyl-CoA variants. *Nat. Chem. Biol.* **13**, 21–29 (2017).
- Zhang, X. Y. et al. SEPT2 crotonylation promotes metastasis and recurrence in hepatocellular carcinoma and is associated with poor survival. *Cell Biosci.* **13**, 63 (2023).
- Liu, S. et al. Chromodomain protein CDYL acts as a crotonyl-CoA hydratase to regulate histone crotonylation and spermatogenesis. *Mol. Cell* **67**, 853–866.e855 (2017).
- Wei, W. et al. Class I histone deacetylases are major histone decrotonylases: evidence for critical and broad function of histone crotonylation in transcription. *Cell Res.* **27**, 898–915 (2017).
- Zhang, J. et al. Crotonylation of GAPDH regulates human embryonic stem cell endodermal lineage differentiation and metabolic switch. *Stem Cell Res. Ther.* **14**, 63 (2023).
- Deng, Q., Ramskold, D., Reinius, B. & Sandberg, R. Single-cell RNA-seq reveals dynamic, random monoallelic gene expression in mammalian cells. *Science* **343**, 193–196 (2014).
- Wang, M., Chen, Z. & Zhang, Y. CBP/p300 and HDAC activities regulate H3K27 acetylation dynamics and zygotic genome activation in mouse preimplantation embryos. *EMBO J.* **41**, e112012 (2022).
- Jiang, G., Li, C., Lu, M., Lu, K. & Li, H. Protein lysine crotonylation: past, present, perspective. *Cell Death Dis.* **12**, 703 (2021).
- Liu, X. et al. The structural basis of protein acetylation by the p300/CBP transcriptional coactivator. *Nature* **451**, 846–850 (2008).
- Wang, F. et al. Histone H2Bub1 deubiquitylation is essential for mouse development, but does not regulate global RNA polymerase II transcription. *Cell Death Differ.* **28**, 2385–2403 (2021).
- Liu, X. et al. Distinct features of H3K4me3 and H3K27me3 chromatin domains in pre-implantation embryos. *Nature* **537**, 558–562 (2016).
- Zhang, B. et al. Allelic reprogramming of the histone modification H3K4me3 in early mammalian development. *Nature* **537**, 553–557 (2016).
- Hsu, H. T. et al. TRANSCRIPTION. Recruitment of RNA polymerase II by the pioneer transcription factor PHA-4. *Science* **348**, 1372–1376 (2015).
- Wang, F., Marshall, C. B. & Ikura, M. Transcriptional/epigenetic regulator CBP/p300 in tumorigenesis: structural and functional versatility in target recognition. *Cell Mol. Life Sci.* **70**, 3989–4008 (2013).
- Chan, S. H. et al. Brd4 and P300 confer transcriptional competency during zygotic genome activation. *Dev. Cell* **49**, 867–881.e868 (2019).
- Hunt, G., Boija, A. & Mannervik, M. p300/CBP sustains Polycomb silencing by non-enzymatic functions. *Mol. Cell* **82**, 3580–3597.e3589 (2022).
- Dahl, J. A. et al. Broad histone H3K4me3 domains in mouse oocytes modulate maternal-to-zygotic transition. *Nature* **537**, 548–552 (2016).
- Liao, P. et al. Crotonylation at serine 46 impairs p53 activity. *Biochem. Biophys. Res. Commun.* **524**, 730–735 (2020).
- Kwon, O. K., Kim, S. J. & Lee, S. First profiling of lysine crotonylation of myofibrillar proteins and ribosomal proteins in zebrafish embryos. *Sci. Rep.* **8**, 3652 (2018).
- Yang, Q. et al. The response of *Rhodotorula mucilaginosa* to patulin based on lysine crotonylation. *Front. Microbiol.* **9**, 2025 (2018).
- Montellier, E., Rousseaux, S., Zhao, Y. & Khochbin, S. Histone crotonylation specifically marks the haploid male germ cell gene expression program: post-meiotic male-specific gene expression. *Bioessays* **34**, 187–193 (2012).
- Li, J. et al. Metabolic control of histone acetylation for precise and timely regulation of minor ZGA in early mammalian embryos. *Cell Discov.* **8**, 96 (2022).
- Li, Y. et al. Molecular coupling of histone crotonylation and active transcription by AF9 YEATS domain. *Mol. Cell* **62**, 181–193 (2016).

43. Xu, W. et al. Global profiling of crotonylation on non-histone proteins. *Cell Res.* **27**, 946–949 (2017).
44. Dang, L. et al. Nuclear condensation of CDYL links histone crotonylation and cystogenesis in autosomal dominant polycystic kidney disease. *J. Am. Soc. Nephrol.* **33**, 1708–1725 (2022).
45. Kelly, R. D. W. et al. Histone deacetylase (HDAC) 1 and 2 complexes regulate both histone acetylation and crotonylation in vivo. *Sci. Rep.* **8**, 14690 (2018).
46. Gao, D. et al. CLAUDIN7 modulates trophectoderm barrier function to maintain blastocyst development in pigs. *Theriogenology* **158**, 346–357 (2020).
47. Picelli, S. et al. Full-length RNA-seq from single cells using Smart-seq2. *Nat. Protoc.* **9**, 171–181 (2014).
48. Kaya-Okur, H. S. et al. CUT&Tag for efficient epigenomic profiling of small samples and single cells. *Nat. Commun.* **10**, 1930 (2019).
49. Trapnell, C. et al. Differential gene and transcript expression analysis of RNA-seq experiments with TopHat and Cufflinks. *Nat. Protoc.* **7**, 562–578 (2012).
50. Martin, M. Cutadapt removes adapter sequences from high-throughput sequencing reads. *EMBnet J.* **17**, 10–12 (2011).
51. Kim, D., Paggi, J. M., Park, C., Bennett, C. & Salzberg, S. L. Graph-based genome alignment and genotyping with HISAT2 and HISAT-genotype. *Nat. Biotechnol.* **37**, 907–915 (2019).
52. Wu, T. et al. clusterProfiler 4.0: a universal enrichment tool for interpreting omics data. *Innovation* **2**, 100141 (2021).
53. Langmead, B. & Salzberg, S. L. Fast gapped-read alignment with Bowtie 2. *Nat. Methods* **9**, 357–359 (2012).
54. Ramirez, F. et al. deepTools2: a next generation web server for deep-sequencing data analysis. *Nucleic Acids Res.* **44**, W160–165, (2016).
55. Zhang, Y. et al. Model-based analysis of ChIP-Seq (MACS). *Genome Biol.* **9**, R137 (2008).
56. Yu, G., Wang, L. G. & He, Q. Y. ChIPseeker: an R/Bioconductor package for ChIP peak annotation, comparison and visualization. *Bioinformatics* **31**, 2382–2383 (2015).

Acknowledgements

This work was supported by the National Key Research and Development Program of China (2021YFA1100302 to Q.Y.S.), and the Shenzhen Science and Technology Program (KQTD20190929172749226 to K.L., Q.Y.S., and W.S.B.Y.).

Author contributions

Di Gao and Chao Li conducted the primary experiments and data analysis. Shao-Yuan Liu and Teng-Teng Xu collected samples and participated in some data analysis. Technical support was provided by Xiao-

Ting Lin, Yong-Peng Tan, Fu-Min Gao and Li-Tao Yi. Di Gao wrote the manuscript with help from all authors. Jian V. Zhang, Jun-Yu Ma, Tie-Gang Meng, William S. B. Yeung and Kui Liu participated in the project discussions. Xiang-Hong Ou, Rui-Bao Su and Qing-Yuan Sun designed the study and revised the manuscript. Qing-Yuan Sun coordinated the research, reviewed, and revised the manuscript. The final manuscript was reviewed and approved by all authors.

Competing interests

The authors declare no competing interests.

Additional information

Supplementary information The online version contains supplementary material available at <https://doi.org/10.1038/s41467-024-50731-0>.

Correspondence and requests for materials should be addressed to Xiang-Hong Ou, Rui-Bao Su or Qing-Yuan Sun.

Peer review information *Nature Communications* thanks Atsuo Ogura and the other anonymous reviewer(s) for their contribution to the peer review of this work. A peer review file is available.

Reprints and permissions information is available at <http://www.nature.com/reprints>

Publisher's note Springer Nature remains neutral with regard to jurisdictional claims in published maps and institutional affiliations.

Open Access This article is licensed under a Creative Commons Attribution-NonCommercial-NoDerivatives 4.0 International License, which permits any non-commercial use, sharing, distribution and reproduction in any medium or format, as long as you give appropriate credit to the original author(s) and the source, provide a link to the Creative Commons licence, and indicate if you modified the licensed material. You do not have permission under this licence to share adapted material derived from this article or parts of it. The images or other third party material in this article are included in the article's Creative Commons licence, unless indicated otherwise in a credit line to the material. If material is not included in the article's Creative Commons licence and your intended use is not permitted by statutory regulation or exceeds the permitted use, you will need to obtain permission directly from the copyright holder. To view a copy of this licence, visit <http://creativecommons.org/licenses/by-nc-nd/4.0/>.

© The Author(s) 2024